Materials and Components
Technology Division
Materials and Components
Technology Division
Materials and Components
Technology Division
Materials and Components
Technology Division

Materials and Components
Technology Division
Materials and Components
Technology Division
Materials and Components
Technology Division

Materials and Components
Technology Division
Materials and Components
Technology Division
Materials and Components
Technology Division
Materials and Components
Technology Division
Materials and Components
Technology Division
Materials and Components
Technology Division
Materials and Components
Technology Division
Materials and Components
Technology Division
Materials and Components
Technology Division

Environmentally Assisted Cracking in Light Water Reactors: Semiannual Report

October 1986–March 1987

by W. J. Shack, T. F. Kassner, P. S. Maiya,
J. Y. Park, and W. E. Ruther

Materials and Components
Technology Division
Materials and Components
Technology Division
Materials and Components
Technology Division
Materials and Components
Technology Division

ARGONNE NATIONAL LABORATORY
9700 South Cass Avenue
Argonne, Illinois   60439

ENVIRONMENTALLY ASSISTED CRACKING IN LIGHT WATER REACTORS:
SEMIANNUAL REPORT

October 1986--March 1987

by

W. J. Shack, T. F. Kassner, P. S. Maiya,
J. Y. Park, and W. E. Ruther

Materials and Components Technology Division

Report Completed
December 1987

Previous Reports in this series

ANL-85-33	October 1983--September 1984
ANL-84-60 Vol. III	October--December 1984
ANL-85-75 Vol. I	January--March 1985
ANL-86-31	April--September 1985
ANL-86-37	October 1985--March 1986
ANL-87-37	April--September 1986

ENVIRONMENTALLY ASSISTED CRACKING IN LIGHT WATER REACTORS:
SEMIANNUAL REPORT

October 1986--March 1987

ABSTRACT

This progress report summarizes work performed by Argonne National Laboratory on environmentally assisted cracking in light water reactors during the six months from October 1986 to March 1987.

TABLE OF CONTENTS

ENVIRONMENTALLY ASSISTED CRACKING IN LIGHT WATER REACTORS:
SEMIANNUAL REPORT[a]

October 1986--March 1987

EXECUTIVE SUMMARY

Fracture-mechanics crack growth rate tests were performed to compare the stress corrosion cracking (SCC) behavior of sensitized Type 304 stainless steel (SS) with that of modified Type 347 SS under the same loading and water chemistry conditions at 289°C. The specimens were subjected to low-frequency, high-R cyclic loading in high-purity water with 0.2 ppm dissolved oxygen as well as in water containing 0.03 and 0.1 ppm sulfate at this oxygen concentration. The results indicated that no crack growth occurred in the modified Type 347 SS specimen over the ~5900-h test duration, whereas the sensitized Type 304 SS specimen cracked intergranularly at rates that were in excellent agreement with previous results under similar water chemistry and loading conditions. Metallographic analyses of the specimens at the conclusion of the experiment confirmed that no stress corrosion cracks initiated at the base of the fatigue crack in the modified Type 347 SS specimen and that intergranular stress corrosion cracking (IGSCC) occurred in the sensitized Type 304 SS specimen, as expected. Metallographic analyses of Type 316NG SS and sensitized Type 304 SS specimens from a previous fracture-mechanics crack growth experiment in simulated boiling-water reactor (BWR) water confirmed the predominately transgranular and intergranular modes of crack propagation in the respective materials.

In a similar experiment, the resistance of Type 304/ER 308L weld metal (used for weld overlay repairs) to SCC was investigated in high-purity water with ~0.2 ppm dissolved oxygen at 289°C. After the crack tip approached the interface with the weld overlay, compliance measurements indicated that no crack growth into the overlay occurred over a time period of ~2100 h at a stress intensity of ~30-33 MPa·m$^{\frac{1}{2}}$ in the high-purity water. Subsequently, sulfate was added to the feedwater (0.01 and 0.03 ppm), and the crack length monitoring systems indicated crack propagation at a slow rate. Metallographic examination of the specimen at the conclusion of the test revealed that during

---

the initial phase in high-purity water, the crack branched at the end of the fatigue precrack in the furnace-sensitized base material near the weld overlay interface and grew within the base material. Subsequently, each branch grew a small distance parallel to the interface and the applied load. This behavior is consistent with that of another specimen exposed to oxygenated water with 0.1 ppm sulfate under similar loading conditions. These observations confirm the inherent resistance of the weld overlay material to SCC in simulated BWR environments.

Constant extension rate tensile (CERT) tests were performed to determine the susceptibility of Types 316NG, modified 347, and solution-annealed 304 SS to transgranular stress corrosion cracking (TGSCC) in 289°C water containing ~0.25 ppm dissolved oxygen and 0.1 ppm sulfate. In these experiments, the effects of weld-induced plastic strain in the specimens, applied strain rate, and heat-to-heat variations in the materials on SCC susceptibility were determined. The results indicated that (1) weld-induced plastic strains had no significant effect on either crack initiation or propagation in Type 316NG SS, (2) the transgranular crack growth rates of Types 316NG and solution-annealed 304 SS were essentially the same under this water chemistry condition, and (3) the TGSCC susceptibility of four heats of Type 316NG SS (produced by Sumitomo) and four heats of modified Type 347 SS was consistently superior to that of our reference heat of Type 316 NG SS. The latter behavior does not appear to be related to the chemical compostion of major alloying elements or the grain size of the different materials. A detailed microstructural evaluation is in progress to determine the presence of second phases and the distribution of minor elements in the materials to elucidate the causes for the variability in resistance to TGSCC. A model that was developed to interpret the effects of strain rate, microstructure and environment on SCC susceptibility of stainless steels in CERT tests was used to estimate the relative contributions of slip-dissolution and slip-oxidation modes of crack advance during IGSCC. The analysis suggests that slip-dissolution is the primary mechanism of cracking of these steels in normal BWR-type water chemistries.

In addition to ionic impurities in BWR coolant systems, corrosion products (viz., insoluble iron and iron oxides) from the feedwater train are transported in the reactor water. In plants with copper alloy condenser tubes

vi

and/or feedwater heaters, copper species are also present. Since corrosion products (e.g., CuO or Cu_2O) can dissolve in high-temperature water, the cations can participate in corrosion reactions. The contribution of oxygen from this source is small in comparison with that from radiolysis of the water. CERT experiments were performed on sensitized Type 304 SS specimens in water containing 0.1 to 20 ppm $CuCl_2$ at a low dissolved-oxygen concentration (<5 ppb) to explore the effect of metallic impurities on the SCC susceptibility at temperatures between 150 and 289°C. At 150°C, IGSCC occurred for feedwater Cu^{2+} concentrations >0.1 ppm, and the crack growth rates increased with cupric ion concentation over the range of ~0.2 to 10.0 ppm. At 200 and 289°C, an abrupt transition from predominately ductile fracture to IGSCC occurred at cupric ion concentrations above ~1 and 2 ppm, respectively, and the crack growth rates were virtually independent of Cu^{2+} concentration at higher values. Electrochemical potential data for Type 304 SS obtained during the CERT experiments indicate that IGSCC does not occur at values below approximately +230, -90, and -290 mV(SHE) at 150, 200, and 289°C, respectively. The effect of pH on the SCC behavior of the material was investigated at 289°C at Cu^{2+} concentrations between 1 and 5 ppm. At cupric ion concentrations that caused severe IGSCC in near-neutral water (viz., 3 and 5 ppm Cu^{2+}), either morpholine ($pH_{25°C}$ = ~6.7 to 8.5) or HCl ($pH_{25°C}$ = ~3.7 to 4.8) additions to the feedwater caused a significant decrease in SCC susceptibility of the steel. The distinct transition from predominately ductile fracture to severe IGSCC over a small concentration range in near-neutral water and the strong effect of pH on SCC susceptibility at a fixed Cu^{2+} concentration may be related to the solubility of various copper species in the water.

Organic impurities and their decomposition products are of concern in BWR and pressurized-water reactor (PWR) secondary-system cooling water in relation to localized corrosion and SCC susceptibility of piping and heat exchanger tube materials. Of the many potential pathways for entry of chemicals used in power plants into the reactor coolant, the make-up water is the major source of organic impurities. The effect of several carboxylic and aliphatic acids on the SCC susceptibility of sensitized Type 304 SS was determined in CERT experiments at 289°C in water containing 0.2 ppm dissolved oxygen and 1.0 ppm of the various acids. These acids have been detected in both BWR and PWR

water at much lower concentrations. The CERT data indicate that the organic
acids are not particularily deleterious compared to other ionic impurities
at the same or lower concentrations in the water. Nevertheless, the
concentrations of organic impurities in reactor water should be minimized
because their decomposition products contribute to the conductivity and
decrease the pH; this could mask the presence of deleterious species (e.g.,
sulfate) in the water.

Finite-element analyses have been performed on a 28-in.-diam weldment to
study the sensitivity of stresses and strains near the weld region produced by
the Mechanical Stress Improvement Process (MSIP), developed by O'Donnell and
Associates, Inc. to variations in the materials properties and the applied
compressive strains. The calculated axial stresses were in reasonable
agreement with measured values, but the values for the hoop stresses were
about one-half the measured values, particularly in the region close to the
weld. The variation of the axial and hoop residual stress distributions with
applied strain was also determined. The analysis indicates that for applied
hoop strains below a threshold value, the final MSIP residual stresses will
depend on the applied strain level and the initial residual stress state in
the weldment. Above this threshold strain level, the MSIP stresses near the
weld are not dependent on the applied strain. Although the threshold strain
level cannot be determined from the present results, the computed plastic
strain levels suggest that strains >1.5% are large enough to overwhelm any
preexisting stresses in the material. The magnitudes of the hoop and axial
stresses on the inner surface of the piping were proportional to the yield
stress of the material, as was expected.

Although operating experience with ferritic steel components in reactor
pressure boundaries is considerably better than that for weld-sensitized
austenitic stainless steels, numerous instances of cracking have occurred.
Work has begun to characterize the environmental and material conditions that
an promote SCC susceptibility in these steels.

ENVIRONMENTALLY ASSISTED CRACKING IN LIGHT WATER REACTORS:
SEMIANNUAL REPORT

October 1986--March 1987

Principal Investigators:
W. J. Shack, T. F. Kassner, P. S. Maiya,
J. Y. Park, and W. E. Ruther

The objective of this program is to develop an independent capability for
the assessment of environmentally assisted cracking in light water reactor
(LWR) systems. During this reporting period, the program has been primarily
directed at problems of intergranular stress corrosion cracking (IGSCC). The
scope of the work includes (1) evaluation of the influence of metallurgical
variables, stress, and the environment on susceptibility to stress corrosion
cracking (SCC), including the influence of plant operations on these
variables; and (2) examination of practical limits for these variables to
effectively control SCC in LWR systems.

The effort during this reporting period has focused on (A) an evaluation
of the SCC of alternate materials and weld overlays, (B) an investigation of
the effects of water chemistry on the SCC of sensitized Type 304 SS, and (C)
an investigation of environmentally assisted cracking of ferritic steels. The
program seeks to evaluate potential solutions to SCC in LWRs by direct
experimentation, through the development of a better understanding of the
various phenomena.

A. Alternate Materials and Weld Overlays

1. Introduction

An evaluation of alternate materials as a generic remedy to
environmentally assisted cracking problems in BWRs is the focus of this
task. Crack growth tests have been performed on Type 316NG and modified 347
stainless steels, which have been used as a replacement for Type 304 SS piping
in BWRs in the U.S. and Japan and as piping material in German BWRs,
respectively.

2. Technical Progress

    a.   Fracture-Mechanics Crack Growth Tests (W. E. Ruther, W. K. Soppet, J. Y. Park, and T. F. Kassner)

    (i)   Comparison of Types 304 and 347 SS in 289°C Water

Fracture mechanics crack growth rate tests were performed to compare the behavior of sensitized Type 304 SS with that of modified Type 347 SS in high-purity water with 0.2 ppm dissolved oxygen and in water containing 0.03 and 0.1 ppm sulfate at this oxygen concentration. As in previous tests, the specimens were fatigue-precracked in air at 289°C to provide 1-mm-deep starter cracks before testing in water began at this temperature. Crack growth was determined from compliance measurements. The tests were conducted under low-frequency, cyclic loading with a positive sawtooth waveform at a frequency of 8×10^{-2} Hz and an R value of 0.95. The stress intensity factors ranged from about 30 to 43 MPa·m$^{\frac{1}{2}}$ for the sensitized Type 304 SS specimen and 28 to 36 MPa·m$^{\frac{1}{2}}$ for the modified Type 347 SS specimen. The results in Table 1 indicate that no crack growth occurred in the Type 347 SS specimen under any of the water chemistry and loading conditions over a time period of ~5900 h. The dependence of the crack growth rate of the lightly sensitized Type 304 SS specimen (EPR = 2 C/cm^2) is in excellent agreement with previous results on this material under the same water chemistry conditions.[1,2] The present data confirm the more extensive CERT results, which indicate that modified Type 347 SS is inherently more resistant to SCC than Type 304 SS in high-temperature water containing dissolved oxygen and sulfate at low concentration.[3,4]

    (ii)   Crack Morphology in Specimens of Types 304 and 316NG SS

The results of a long-term crack-growth experiment on Types 304 and 316NG SS over a range of water chemistry and loading conditions were presented in the previous report.[5] The compact tension (1TCT) specimens were sectioned vertically, and half of each section was split in the plane of the crack at liquid-nitrogen temperature to reveal the fracture surface. The corrosion product film was removed from the fracture surface by the APAC process[6,7] [i.e., by exposure of the specimens for 2 h in a gently boiling alkaline permanganate solution (20% NaOH, 3% KMnO$_4$), a hot rinse, and then 2 h

Table 1. Crack Growth Results for Sensitized Type 304 and Type 347 SS Specimens[a] during an Experiment[b] at 289°C in Which the Sulfate Concentration of the Feedwater, Containing 0.2-0.3 ppm Dissolved Oxygen, Was Increased from 0 to 0.1 ppm

Test Cond.	Test Time, h	Water Chemistry				Electrode Potentials		Type 304 SS		Type 347 SS	
		Oxygen, ppm	Hydrogen, ppm	Sulfate, ppm	Cond., μS/cm	304 SS, mV(SHE)	Pt, mV(SHE)	K_{max}[c] MPa·m$^{1/2}$	Growth Rate, m·s^{-1}	K_{max}[c] MPa·m$^{1/2}$	Growth Rate, m·s^{-1}
1	5 2400	0.2-0.3[d]	-	0	0.21	95	110	29.7	1.7×10^{-10}	28.0	~0
2	2400 4247	0.2-0.3[d]	-	0.03	0.35	85	90	32.1	2.2×10^{-10}	28.0	~0
3	4247 5231	0.2-0.3[d]	-	0.1	0.93	65	65	34.3	4.4×10^{-10}	28.0	~0
4	5281 5749	0.2-0.3[d]	-	0.1	0.93	115	130	42.6	8.0×10^{-10}	32.0	~0
5	5749 5917[e]	0.2-0.3[d]	-	0.1	0.93	115	130	e	e	36.0	~0

[a]Compact tension specimens (0.75 TCT) of Type 304 SS (Heat No. 30956) and Type 347 SS (Heat No. K2B1) with the following heat treatments: solution anneal at 1050°C for 0.5 h, followed by 760°C for 0.25 h plus 500°C for 24 h for the Type 304 SS specimen (EPR = 2 C/cm^2), or 650°C for 24 h for the Type 347 SS specimen (EPR = 0 C/cm^2).

[b]The frequency of the positive sawtooth waveform was 8×10^{-2} Hz, and the load ratio was 0.95.

[c]Stress intensity, K_{max}, at the end of the test condition.

[d]Effluent dissolved-oxygen concentration; feedwater oxygen concentration at the 0.2-0.3 ppm level was higher by approximately a factor of two to compensate for oxygen depletion by corrosion of the autoclave system.

[e]Test terminated because the crack opening of the Type 304 SS specimen exceeded the range of the clip gage.

3

in a dibasic ammonium citrate solution) to reveal the morphology of the underlying material. The intact portion of the specimens that encompassed the crack was polished and etched to corroborate the mode of crack propagation and also to determine if macrobranching of the crack had occurred during the test. In addition, the total crack lengths at the end of the test were measured and found to be in agreement with the values obtained from the clip gages.

The micrographs in Fig. 1 indicate that the crack path and fracture surface morphology of the sensitized Type 304 SS specimen were intergranular, as in previous specimens.[8,9] The corresponding micrographs for the Type 316NG SS specimen in Fig. 2 indicate that the mode of crack propagation was predominately transgranular; however, there is some evidence of intergranular microbranching off the main crack and in the crack tip region. TGSCC is invariably the mode of crack propagation in this material during CERT experiments.[10,11] Figure 3 shows the crack fronts from the outer edge to the half-thickness (B/2) in the two specimens. As in previous specimens of sensitized Type 304 SS, the crack front exhibits considerable curvature, i.e., greater stress corrosion propagation near the edge of the specimen (a reverse thumb-nail crack),[8,9] whereas the crack front of the Type 316NG SS specimen progressed uniformily into the material with minimal edge effects.

Figure 4 shows similar micrographs of specimens in which the crack growth behavior of Types 304 and modified 347 SS was compared. The mode of crack propagation in the lightly sensitized Type 304 SS was intergranular, as in all previous instances. No SCC at the base of the fatigue precrack is evident in the polished and etched transverse section of the modified Type 347 SS specimen. This observation is consistent with compliance measurements from the clip gage during the experiment, which indicated that no crack growth had occurred.

(iii) Type 304/308L Weld Overlay

To characterize the inherent crack growth resistance of the Type 308L weld metal used for weld overlay repairs, crack growth experiments were performed on a fracture-mechanics-type specimen fabricated

LOADING CONDITIONS

Kmax= 28-38.9 MPa·m$^{1/2}$

FREQUENCY=0.08 Hz

R =0.95

SENSITIZATION

EPR=2 C/cm^2

TEMPERATURE

289-200°C

TRANSVERSE SECTION   ENTIRE CRACK AT D/2   FRACTURE SURFACE
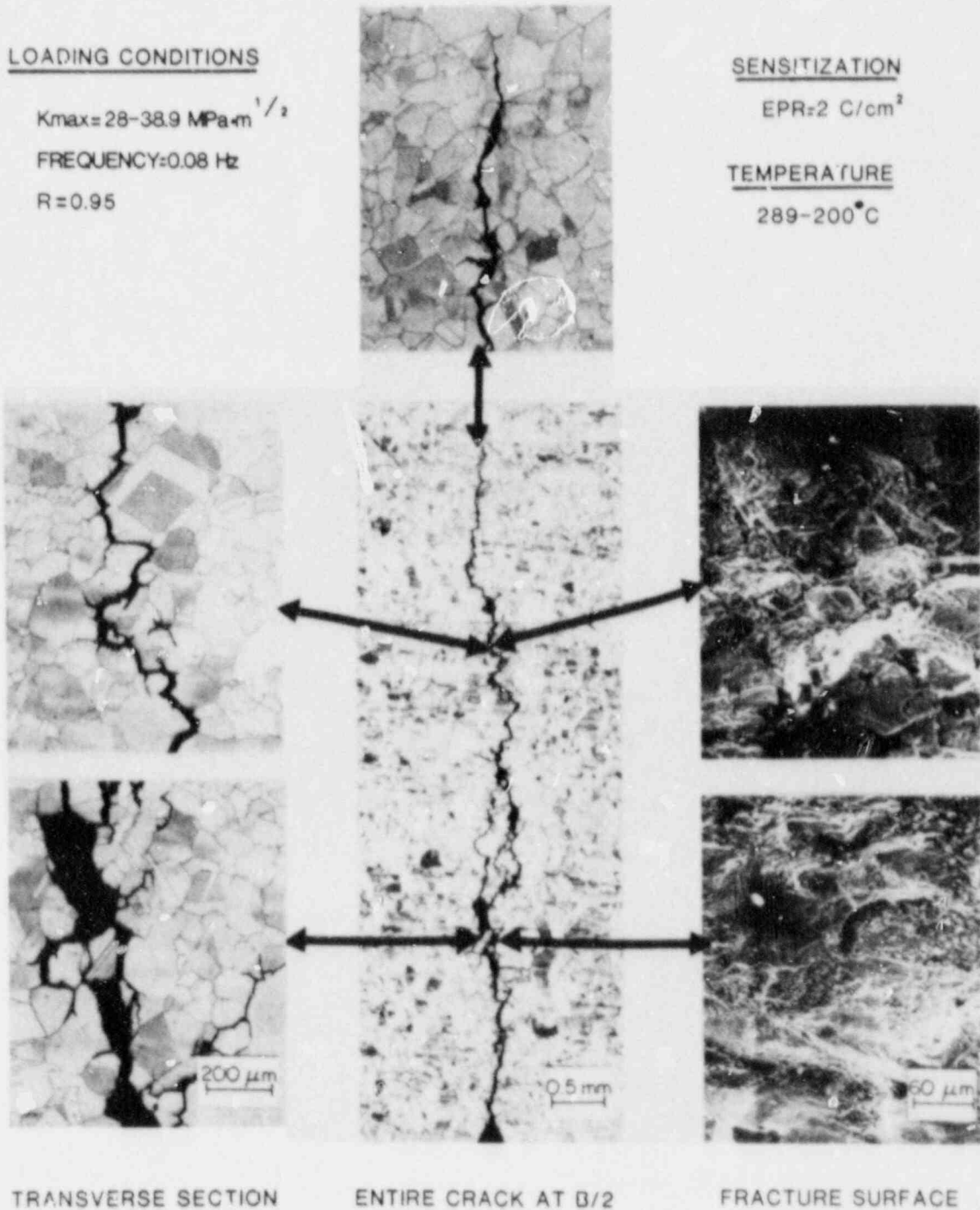
Fig. 1. Crack Path and Fracture Surface Morphology of a Lightly
Sensitized Type 304 SS Specimen (No.23, Heat No. 30956)
after a Crack Growth Experiment under Low-Frequency Cyclic
Loading in 200 and 289°C Water with Different Simulated
BWR Water Chemistry Conditions.

6

0.5 mm

ENTIRE CRACK AT B/2

200 μm

60 μm

TRANSVERSE SECTION
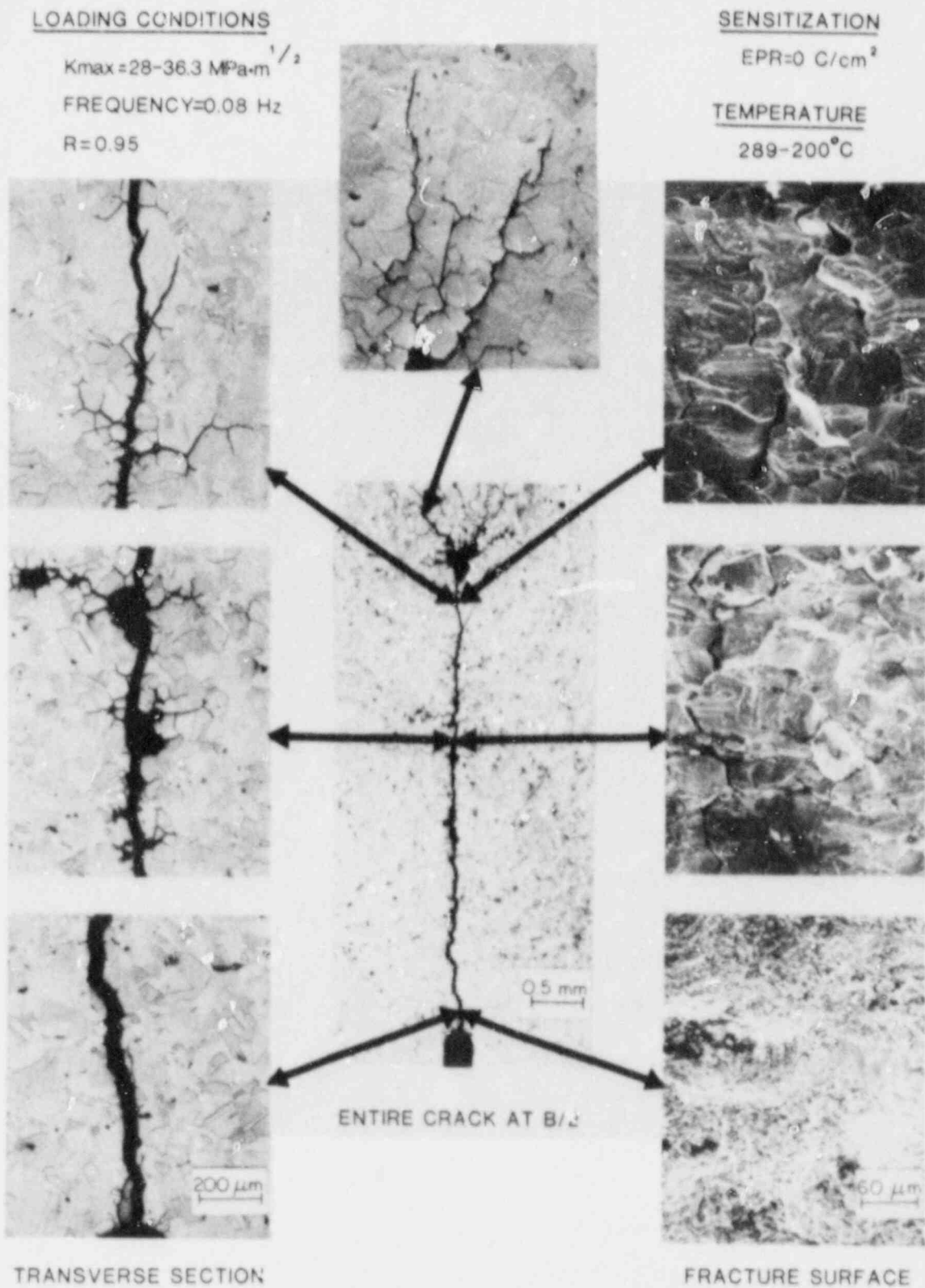
FRACTURE SURFACE

Fig. 2. Crack Path and Fracture Surface Morphology of a Type 316NG SS Specimen (No. E-01, Heat No.91576) after a Crack Growth Experiment under Low-Frequency Cyclic Loading in 200 and 289°C Water with Different Simulated BWR Water Chemistry Conditions.
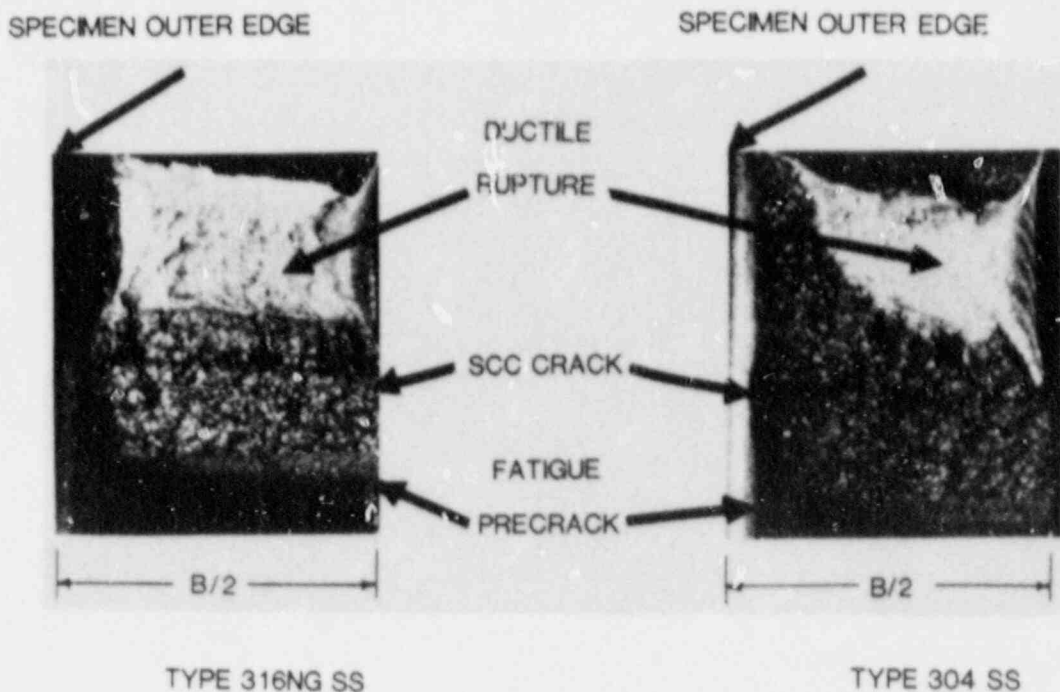
Fig. 3. Crack Fronts in the Types 304 and 316NG SS Specimens from
the Crack Growth Experiment after Simultaneous Exposure to
Low-Frequency Cyclic Loading under Simulated BWR Water
Chemistry Conditions at 200 and 289°C.

from a 10-in.-diam Schedule 140 Type 304 SS pipe with a weld overlay designed
by NUTECH Engineers and applied by GAPCO Welding in accordance with their
standard overlay repair procedure. The compact tension (1TCT) specimen was
designed so that the crack propagates through the base material and into the
Type 308L SS overlay. The base material was furnace-sensitized at 600°C for
24 h, which produced an EPR value of 28 C/cm^2, before the overlay was
applied. The ferrite content of the overlay was 12 ± 0.5%, as measured by a
ferrite scope. The composition of the pipe and overlay material was presented
in a previous report.[12] The crack growth experiments were performed in high-
purity water with 8 ppm dissolved oxygen at 289°C under a cyclic load with an
R value of 0.9, a frequency of 2×10^{-3} Hz, and an initial maximum stress
intensity K_{max} of 28 MPa·m$^{\frac{1}{2}}$. The crack length was measured by compliance and
a.c. potential drop techniques. During the initial 2231 h of testing, the
changes in compliance and potential drop measurements indicated that the crack
was growing at an average rate of 2×10^{-10} m·s^{-1} in the sensitized base metal
and that the crack tip was near the interface with the weld overlay.
Subsequently, a feedwater pump failure occurred, and the system was shut

LOADING CONDITIONS

Kmax(347)=28 MPa·m$^{1/2}$

Kmax(304)=30-43 MPa·m$^{1/2}$

FREQUENCY=0.08 Hz

R=0.95

WATER CHEMISTRY

OXYGEN 0.2-0.3ppm

SULFATE 0-0.1 ppm

SENSITIZATION

EPR(347)=0 C/cm^2

EPR(304)=2 C/cm^2

TYPE 304 SS

FRACTURE SURFACE

OUTER EDGE OF SPECIMEN

— DUCTILE RUPTURE

— SCC

— FATIGUE CRACK

|← B/2 →|

TYPE 304 SS

CRACK FRONT

TYPE 347 SS

FATIGUE PRECRACK

NO SCC DURING TEST

TYPE 304 SS

CRACK TIP AT B/2
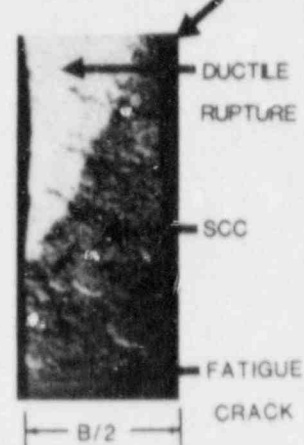
Fig. 4. Micrographs of the Initial Fatigue Crack in a Modified Type 347 SS Specimen (No. K2B1, Heat No. 316642) and the Intergranular Stress Corrosion Crack in a Lightly Sensitized Type 304 SS Specimen (No.22, Heat No. 30956) after Simultaneous Exposure to Low-Frequency Cyclic Loading under Simulated BWR Water Chemistry Conditions at 289°C.

down. The test resumed after repair of the pump, but no crack growth was observed in the ensuing 1400-h period. It is not clear whether this was due to the interruption of the test (previous experience suggests that an incubation period of 500-1000 h can be expected after such an interruption) or whether it was indicative of the inherent crack growth resistance of the weld-overlay material in a high-purity environment.

The stress intensity was increased in an effort to restart crack growth. However, no crack growth was observed during a test period of 840 h at K_{max} = 30 MPa·m$^{1/2}$ and during a subsequent 1296-h test period at K_{max} = 33 MPa·m$^{1/2}$. The test was continued after 0.01 and 0.03 ppm sulfate was

added to the oxygenated feedwater. Changes were noted in both the compliance and potential drop measurements in these environments, and the apparent average crack growth rate was 7×10^{-11} m·s^{-1} at $K_{max} = 33$ MPa·m$^{\frac{1}{2}}$. However, posttest examination of the specimen revealed that the changes in the compliance and potential drop measurements during the period after the crack tip reached the weld overlay interface were not due to crack growth in the overlay. As is shown in Fig. 5, the initial stress corrosion crack branched at the base of the fatigue precrack and grew in the furnace-sensitized base material to near the weld interface. Subsequently, each branch grew about 3 mm parallel to the interface and applied load. The mode of cracking was intergranular (Fig. 6). Despite the fact that the material was heavily sensitized, crack growth along the interface apparently occured at measurable rates only in impurity environments. The crack growth behavior in this test is consistent with that obtained on another specimen tested in an impurity environment.[5] These observations confirm the inherent resistance of the weld overlay material to stress corrosion crack growth in simulated BWR environments.

Fig. 5. Cross Section of a 1TCT Weld Overlay Specimen Showing Crack Branching and Propagation in the Base Material near the Weld Fusion Line.
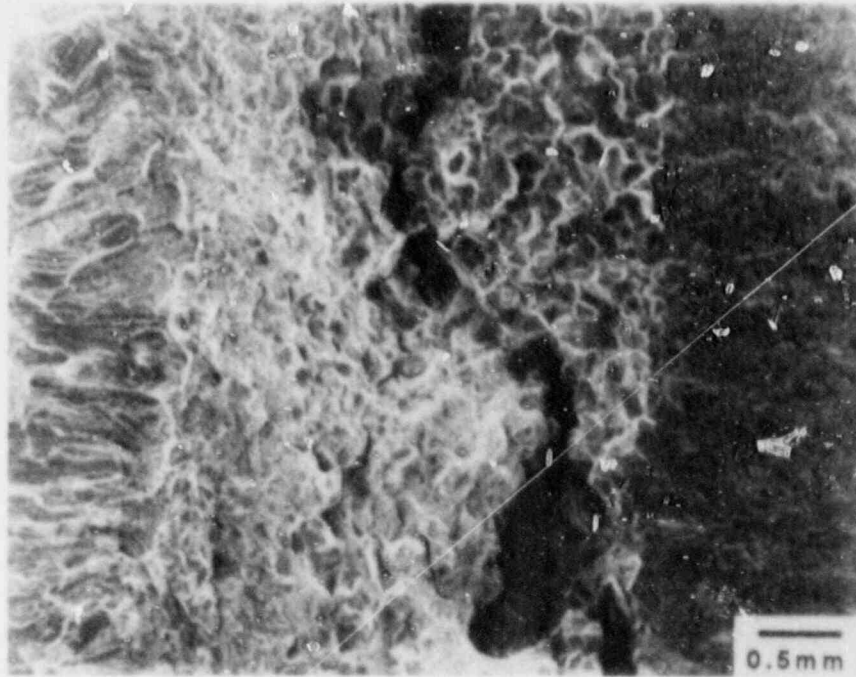
Fig. 6. Fracture Surface of 1TCT Weld Overlay Specimen Showing a
Branched Intergranular Crack in the Base Material.

b. Constant Extension Rate Tests (P. S. Maiya)

(i) Effect of Weld-Induced Plastic Strains on SCC of Type 316NG SS

Previous tests[11] on CERT specimens of Type 316NG SS fabricated
from a 28-in.-diam pipe weldment obtained from the EPRI NDE Center showed that
crack initiation was not affected by weld-induced plastic strains. However,
the crack growth rates were somewhat higher than those observed in
corresponding tests on our reference heat (No. P91576) of Type 316NG SS. To
determine whether this variation is simply due to heat-to-heat variability or
represents a real effect of weld cold work, comparison tests were performed on
base material obtained away from the weld region. The specimens were heat-
treated at 1050°C for 0.5 h plus 650°C for 24 h prior to testing. The tests
were performed in water containing 0.25 ppm dissolved oxygen and 0.1 ppm
sulfate (added as acid) over a range of strain rates. The results obtained
from specimens free from weld-induced plastic strains (specimen Nos. NDE-28-B1
and -B2) at strain rates of 5×10^{-7} and 2×10^{-7} s^{-1} are shown in Table 2,

Table 2. Comparison of CERT Test Results for Type 316NG SS 28-in.-diam Pipe Weldment with[a] and without[b] Weld-Induced Plastic Strains. $T = 289°C$. Environment: 0.25 ppm Oxygen with 0.1 ppm Sulfate. Water Conductivity: 0.9 $\mu S/cm$

Specimen No.	$\dot{\epsilon}$, s^{-1}	t_{ℓ}, h	ϵ_f, %	$\Delta A/A_o$, %	σ_{max}, MPa	$\dot{a}_{av}$, $m \cdot s^{-1}$	SS Potential, mV(SHE)
NDE-28-1[a]	1×10^{-6}	68	24.7	67	474	-	42
NDE-28-2[a]	4×10^{-7}	166	24.0	61	478	2.06×10^{-9}	52
NDE-28-B1[b]	5×10^{-7}	247	44.6	-	465	3.61×10^{-9}	37
NDE-28-3[a]	2×10^{-7}	349	25.1	66	487	1.52×10^{-9}	137
NDE-28-B2[b]	2×10^{-7}	653	47.0	52	470	1.28×10^{-9}	40
316NG[c]	2×10^{-7}	474	34.0	44	461	7.35×10^{-10}	-
NDE-28-4[a]	1×10^{-7}	688	24.8	53	485	6.06×10^{-10}	32

[a]Type 316NG SS from 28-in.-diam pipe with weld-induced plastic strains.
[b]Type 316NG SS from 28-in.-diam pipe without weld-induced plastic strains.
[c]ANL reference Heat No. P91576 of Type 316NG SS (base).

together with some selected results obtained from specimens with weld-induced plastic strains (specimen Nos. NDE-28-1 to -4). The results reported previously[11] together with those shown in Table 2 suggest that at least from CERT test data, the weld-induced cold work in large-diameter welded pipe has no significant effect on either crack initiation or crack growth.

(ii) Comparison of TGSCC in Types 316NG and Solution-Annealed 304 SS

In CERT tests, Type 316NG SS becomes susceptible to TGSCC at strain rates between 2×10^{-8} and 1×10^{-6} s^{-1}. Tests have been carried out to verify that solution-annealed Type 304 SS is also susceptible to TGSCC under similar conditions. The results of the tests are summarized in Table 3 and are shown in Fig. 7. The crack growth rates for low-carbon Type 316NG SS (ANL reference Heat No. P91576) and the solution-annealed Type 304 SS (Heat

Table 3. Comparison of TGSCC between Type 316NG SS (Heat P91756) and Solution Annealed Type 304 SS (Heat 53319). CERT results in impurity environments (0.25 ppm O_2 + 0.1 ppm SO_4^{2-}). T = 289°C

Test No.	Material	$\dot{\epsilon}$, s^{-1}	t_f, h	σ_{max}, MPa	ϵ_f, %	ϵ_u, %	$\Delta A/A_o$, %	Failure Mode	$\dot{a}_{av}$, $m \cdot s^{-1}$
159	316NG	2×10^{-6}	53.5	453	38.5	32.3	67	Ductile	–
180	304	2×10^{-6}	57.4	500	41.3	35.2	76	Ductile	–
160	316NG	1×10^{-6}	100.6	450	35.9	29.6	65	TGSCC	1.51×10^{-9}
177	304	1×10^{-6}	118.3	500	42.6	37.0	73	TGSCC	1.70×10^{-9}
169	316NG	4×10^{-7}	217.4	462	31.3	29.0	59	TGSCC	9.74×10^{-10}
174	304	4×10^{-7}	288.5	507	41.5	36.4	43	TGSCC	1.11×10^{-9}
172	316NG	2×10^{-7}	474.0	461	34.1	29.8	44	TGSCC	7.35×10^{-10}
175	304	2×10^{-7}	472.7	488	34.0	31.2	41	TGSCC	9.10×10^{-10}
148	316NG	1×10^{-7}	565.9	472	20.3	18.8	61	TGSCC	6.73×10^{-10}
181	304	1×10^{-7}	680.0	481	24.5	21.0	22	TGSCC	7.45×10^{-10}
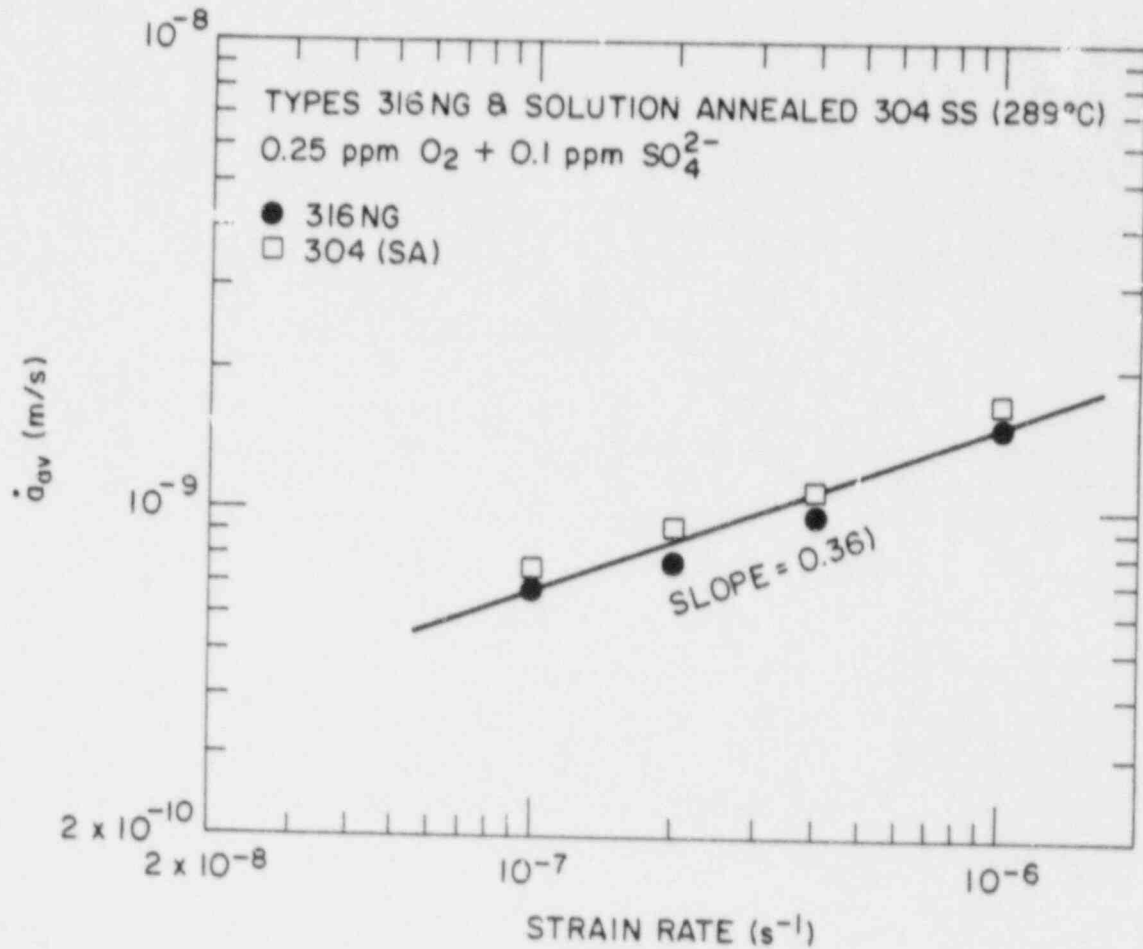
Fig. 7. Comparison of Average Transgranular Crack Growth Rates
for Types 316NG and Solution-Annealed 304 SS.

No. 53319) are approximately the same. The variation in the transgranular
crack growth rate, $\dot{a}_{av}$ in m·s^{-1}, with strain rate for both materials in water
containing sulfate can be described by

$$\dot{a}_{av} = 2.15 \times 10^{-7}(\dot{\epsilon})^{0.36}. \tag{1}$$

Both materials have approximately the same value for the critical strain
rate ($\sim 10^{-6}$ s^{-1}), the strain rate above which cracking does not occur. These

crack growth rates for Types 316NG and solution-annealed 304 SS are consistent with those obtained in fracture-mechanics tests.[13]

(iii) Heat-to-Heat Variation Effects on TGSCC of Types 316NG and 347 SS

SCC tests have been performed on four heats of Type 316NG and four heats of modified Type 347 SS as part of a study on heat-to-heat variations in TGSCC susceptibility. Such variations can arise from differences in grain size, the presence of second phases that can affect the plastic deformation process (for example, the difficulty with which planar slip occurs), or the chemical composition in terms of either the major alloying or residual elements.

The chemical compositions of Type 316NG SS (produced by Sumitomo) and modified Type 347 SS are shown in Table 4. The welded specimens of modified Type 347 were heat-treated at 500°C for 24 h, and the base metal specimens of Types 316NG and modified Type 347 SS were heat-treated at 1050°C for 0.5 h plus 650°C for 24 h. Measurements of grain size were made on several photomicrographs of metallographically prepared, heat-treated specimens by using the intercept method described by Hilliard.[14] The results are given in Table 5. The variations in chemical composition and grain size of the Sumitomo heats of Type 316NG SS are very small. Those for the modified Type 347 SS are more significant.

CERT experiments were conducted in water (289°C) containing ~0.25 ppm dissolved oxygen and 0.1 ppm sulfate added as acid at strain rates between 1×10^{-7} and 1×10^{-6} s^{-1}. The results are presented in Tables 6 and 7. In general, the Sumitomo heats were consistently superior to our reference heat of Type 316NG SS. For example, the transgranular crack growth rates observed for Heat No. D440104 are lower by a factor of 2 than those for our reference heat and lower by a factor of ~4 than those for base material from another Sumitomo heat supplied to us by the EPRI NDE Center in the form of 28-in.-diam pipe. Another Sumitomo heat (No. D442604) was even more resistant, and no TGSCC was observed even at the slowest strain rate. Because these heats of material exhibited very little variation in chemical composition and grain size, the reasons for the variations in resistance to TGSCC are not clear at this time.

Table 4. Chemical Composition (wt.%) of Different Heats of Types 316NG (Sumitomo) and Modified 347 SS

Material	Heat No.	C	Mn	P	S	Si	Ni	Cr	Mo	Cu	N	B	Nb	Fe
316NG	D440104	0.015	1.75	0.011	0.002	0.49	13.25	17.91	2.48	0.12	0.098	–	–	Balance
316NG	D442609	0.014	1.66	0.018	0.002	0.46	12.85	17.29	2.52	–	0.10	–	–	
316NG	D450905	0.019	1.67	0.016	0.002	0.47	13.08	17.43	2.59	0.05	0.10	0.005	–	
316NG	D472701	0.012	1.68	0.014	0.002	0.45	13.35	17.41	2.30	0.07	0.098	0.0008	–	
347	174100	0.023	1.70	0.036	0.015	0.33	11.00	18.15	0.48	0.12	0.029	0.005	0.44	
347	174102	0.03	1.70	0.012	0.019	0.43	10.75	18.53	0.35	0.11	0.021	0.0005	0.51	
347	669962	0.04	1.56	0.017	0.002	0.46	9.69	18.34	0.18	0.05	0.019	0.0002	0.60	
347	316642	0.03	1.56	0.018	0.014	0.29	10.81	18.06	0.29	0.09	0.021	0.0009	0.60	

25

Table 5. Grain Size Distribution Among Different Heats
of Types 316NG (Sumitomo) and Modified 347 SS

Type	Heat	Grain Diam, μm	ASTM No.
316NG	D440104	97	3.4
316NG	D442604	83	3.8
316NG	D450905	81	3.9
316NG	D479701	92	3.5
347	174100	31	6.6
347	1740162	87	3.7
347	869962	16	8.5
347	316642	43	5.8

The TGSCC susceptibility of two heats of Type 347 SS (Heat Nos. 174100 and 170162) has been discussed in a previous report.[3] Additional CERT results have been obtained on two other heats (Nos. 869967 and 316642) of modified Type 347 SS; they are summarized in Table 7 along with the previously reported results. The tests were performed in oxygenated water (0.25 ppm dissolved oxygen) with 0.1 ppm sulfate. All the materials were more resistant to TGSCC than our reference heat of Type 316NG SS, and the crack growth rates were generally lower than those for most of the Sumitomo heats of Type 316NG SS. Heat No. 316642 (supplied by the New York Power Authority) exhibited no cracking under any of the test conditions.

Resistance to crack growth does not appear to be related to grain size or minor changes in chemical composition. An explanation of this variability may require a more detailed examination of the microstructure, especially for the presence of second phases and unidentified trace elements that have not received sufficient attention in the past. We have begun an examination of the microstructure of the four heats of Type 347 SS. Specimens were mechanically polished and electrolytically etched in 10% oxalic acid and

Table 6. CERT Test Results for Four Sumitomo Heats of Type 316NG SS.
Environment: 0.25 ppm O_2 + 0.1 ppm SO_4^{2-}, $T = 289°C$

Test No.	Heat No.	$\dot{\epsilon}$, s^{-1}	t_f, h	σ_{max}, MPa	ϵ_f, %	ϵ_u, %	$\Delta A/A_o$, %	Failure Mode	$\dot{a}_{av}$, $m \cdot s^{-1}$	SS Potential, mV(SHE)
346	D440104	1×10^{-6}	134	452	48.2	40.3	80	Ductile	–	12
347	D440104	5×10^{-7}	266.5	458	48.0	42.5	70	TGSCC	4.51×10^{-10}	54
345	D440104	2×10^{-7}	712.0	464	51.0	44.9	71	TGSCC	3.49×10^{-10}	130
353	D442604	5×10^{-7}	266.5	458	48.0	4.0	79	Ductile	–	45
351	D442604	2×10^{-7}	669.0	463	48.2	43.0	73	Ductile	–	72
354	D450905	5×10^{-7}	269.5	458	48.5	41.6	77	TGSCC	4.75×10^{-10}	35
352	D450905	2×10^{-7}	664.0	468	47.8	40.6	70	TGSCC	7.41×10^{-11}	62
359	D472701	2×10^{-7}	647.0	455	46.6	40.8	65	TGSCC	2.97×10^{-10}	25

17

Table 7. CERT Test Results for Four Heats of Modified 347 SS.
Environment: 0.25 ppm O_2 + 0.1 ppm SO_4^{2-}. T = 289°C

Test No.	Heat No.	$\dot{\varepsilon}$, s^{-1}	t_f, h	σ_{max}, MPa	ε_f, %	ε_u, %	$\Delta A/A_o$, %	Failure Mode	$\dot{a}_{av}$, $m \cdot s^{-1}$	SS Potential, mV(SHE)
263	174100	1×10^{-6}	65.5	432	23.6	18.2	65	Ductile	–	21
274	174100	5×10^{-7}	114.5	417	20.6	16.6	47	TGSCC	1.63×10^{-9}	94
272	174100	2×10^{-7}	301.5	448	21.7	17.8	40	TGSCC	1.10×10^{-9}	-8
275	174100	1×10^{-7}	574.5	451	20.7	16.4	47	TGSCC	7.58×10^{-10}	55
301	170162	1×10^{-6}	55.7	427	20.1	15.1	76	Ductile	–	84
305	170162	5×10^{-7}	114.1	430	20.5	15.5	67	Ductile	–	91
310	170162	2×10^{-7}	250.5	471	18.0	11.7	61	TGSCC	5.50×10^{-10}	22
349	869962	1×10^{-6}	94.5	460	34.0	27.0	61	Ductile	–	22
350	869962	5×10^{-7}	182.8	466	32.9	29.2	55	TGSCC	3.81×10^{-10}	34
348	869962	2×10^{-7}	442.0	472	31.8	28.2	50	TGSCC	2.97×10^{-10}	80
364	316642	1×10^{-6}	100.0	438	36.0	28.8	59	Ductile	–	-1
365	316642	5×10^{-7}	198.0	444	35.6	30.1	63	Ductile	–	3
367	316642	2×10^{-7}	487.0	443	35.1	28.8	55	Ductile	–	-87

18

were examined by means of scanning electron microscopy. Fine niobium-rich precipitates were observed (presumably NbC), especially in the heats exhibiting enhanced resistance to TGSCC, but more work must be done before any conclusions can be drawn. Mechanistically, the precipitation of second phases, particularly at stacking faults, is known to inhibit planar slip, which could increase resistance to TGSCC.

(iv) Strain Rate Effects on SCC

We have presented a model[10,15,16] for the interpretation of strain rate and environmental and microstructural effects on SCC susceptibility observed in CERT tests. The model was based on the assumption that the strain rate near the crack tip strain rate can be estimated by use of a J-integral approach. The crack tip strain rate was then related to crack growth rate by a slip-dissolution model proposed by Ford.[17] Failure of the specimen was described by a J-integral fracture criterion. The model predicts that the average crack growth rate is proportional to the 1/3 power of the nominal strain rate, $(\dot{\epsilon})^{1/3}$. This prediction has been substantiated by CERT results on austenitic stainless steels for both TGSCC and IGSCC in oxygenated water with and without impurities. Experiments are in progress to determine whether the TGSCC observed for Type 304 SS in simulated hydrogen-water chemistry is environmentally assisted and whether a similar relation between strain rate and crack growth rate is valid. The slip-dissolution model in our previous work predicts that the instantaneous crack growth rate is proportional to the 1/2 power of the instantaneous crack tip strain rate. However, recent work has shown that the explicit power law relationships among the nominal and crack tip strain rates and SCC parameters from CERT tests are consistent with several other diffusion-controlled mechanisms that may contribute to crack advance.

For example, we can consider crack advance by a slightly different mechanism, which is described as slip-oxidation. In this case it is assumed that no barrier to oxide nucleation exists at the crack tip exposed to the environment and that crack advance occurs solely by oxide rupture without bare metal dissolution. A schematic representation of the crack tip region is shown in Fig. 8. Crack growth occurs as a result of the interface movement,
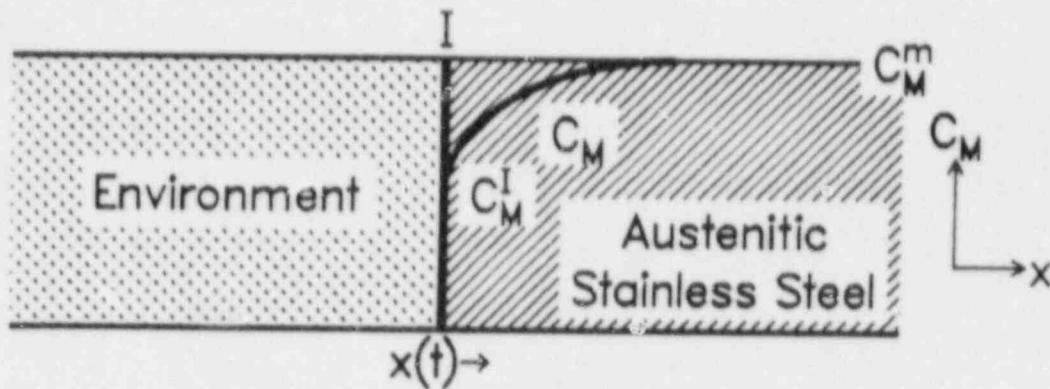
Fig. 8. Schematic View of a Crack Tip Region Exposed to an
Aqueous Environment.

which is assumed to be diffusion-controlled in the austenite matrix. C_M is
the concentration of the diffusing metal, C_M^I is the concentration at the
interface with the environment, and C_M^m is the concentration in the base
metal. The flux J_M^I at the interface divided by the concentration at the
interface J_M^I/C_M^I gives the rate of advance of the interface, i.e., the crack
growth rate $\dot{a}$.

$$\dot{a} = J_M^I/C_M^I \tag{2}$$

The concentration function describing the metal distribution is given by the
diffusion equation

$$\frac{C_M - C_M^I}{C_M^m - C_M^I} = 1 - \mathrm{erf}\left(\frac{X}{2\sqrt{Dt}}\right) \tag{3}$$

where D is the diffusivity of the rate-controlling species and t is the
time. The concentration gradient at the interface is obtained by
differentiating the above equation.

$$\left(\frac{\partial C_M}{\partial X}\right)_I = \frac{C_M^m - C_M^I}{\sqrt{\pi D t}} \exp\left(-\frac{X^2}{4Dt}\right) \tag{4}$$

Relating $(\partial C_M/\partial X)_I$ to J_M^I by Fick's law, an explicit expression for the crack growth rate is obtained in terms of D, t, and a concentration term

$$\dot{a} = \frac{J_M^I}{C_M^I} = \frac{D\left[\frac{\partial C_M}{\partial X}\right]_I}{C_M^I} = \left[\frac{D}{\pi t}\right]^{0.5}\left(\frac{C_M^m - C_M^I}{C_M^I}\right). \tag{5}$$

Identifying the time t with periodicity of oxide rupture, we can derive an expression for an average crack growth rate

$$\dot{a}_{av} = \frac{C_M^m - C_M^I}{C_M^I}\left[\frac{D}{\pi \epsilon_f}\right]^{0.5}(\dot{\epsilon}_T)^{0.5} \tag{6}$$

where ϵ_f = fracture strain of the oxide. The dependence of the average crack growth rate on the crack tip strain rate is identical to that obtained from the slip-dissolution model. Thus our model is also consistent with this mechanism. Furthermore, if oxide film formation were rate limiting for other mechanisms such as hydrogen embrittlement, the power law relationships we have derived would also be consistent with these mechanisms.

Although the form of the equation is similar for both mechanisms, comparisons between experimental results and quantitative estimates of the actual terms may be useful in assessing relative contributions of different mechanisms.

The model parameter A_T is related to the crack length a_f and time at failure t_f by

$$A_T = a_f[6(t_f - t_o)]^{0.5} \tag{7}$$

where t_o is the crack initiation time, which is usually small compared to t_f in CERT tests. The crack growth rate and crack tip strain rate are related by

$$\frac{da}{dt} = (A_{sd}, A_{so}) \dot{\epsilon}_T^{0.5} \tag{8}$$

where the magnitudes of A_{sd} and A_{so} describe the contributions to crack growth by slip-dissolution and slip-oxidation mechanisms, respectively. A_{sd} has been determined by Ford[17] as

$$A_{sd} = \frac{M}{n\rho F} \frac{i_o t_o^{0.5}}{\epsilon_f^{0.5}} \tag{9}$$

where M is the atomic weight of iron; ρ is the density of iron at the temperature of interest; n is the valency change during the oxidation process; i_o is the current density following oxide rupture at $t = t_o$, which corresponds to the bare metal dissolution rate; F is Faraday's constant; and ϵ_f is the fracture strain of the oxide. By using the available data for these variables,[17] A_{sd} can be computed for Type 304 SS in oxygenated water containing 0.2 ppm dissolved oxygen and 0.01 M sodium sulfate; this value is ~2.5 x 10^{-6} m·s$^{-\frac{1}{2}}$.

For the slip-oxidation model, the concentration term $(C_M^m - C_M^I)/C_M^I$ is between 0.4 and 0.5. D is interpreted as the pipe diffusivity of either Fe or Cr. Values of A_{so} based on estimates[18] of the diffusivity are shown in Fig. 9 along with an estimate of A_{sd} and values of A_T obtained from CERT tests on Type 304 SS for different dissolved-oxygen levels with and without impurities.[19] The smaller value for pipe diffusivity is based on published data for iron,[18] and the value for the diffusivity of Cr should not be vastly different. The larger value of D was obtained somewhat arbitrarily by increasing the literature value by an order of magnitude to account for uncertainties and to obtain an upper bound for the expected contribution of the slip-oxidation process. Despite the uncertainty associated with some of the values used in determining values of A for specific mechanisms, our model
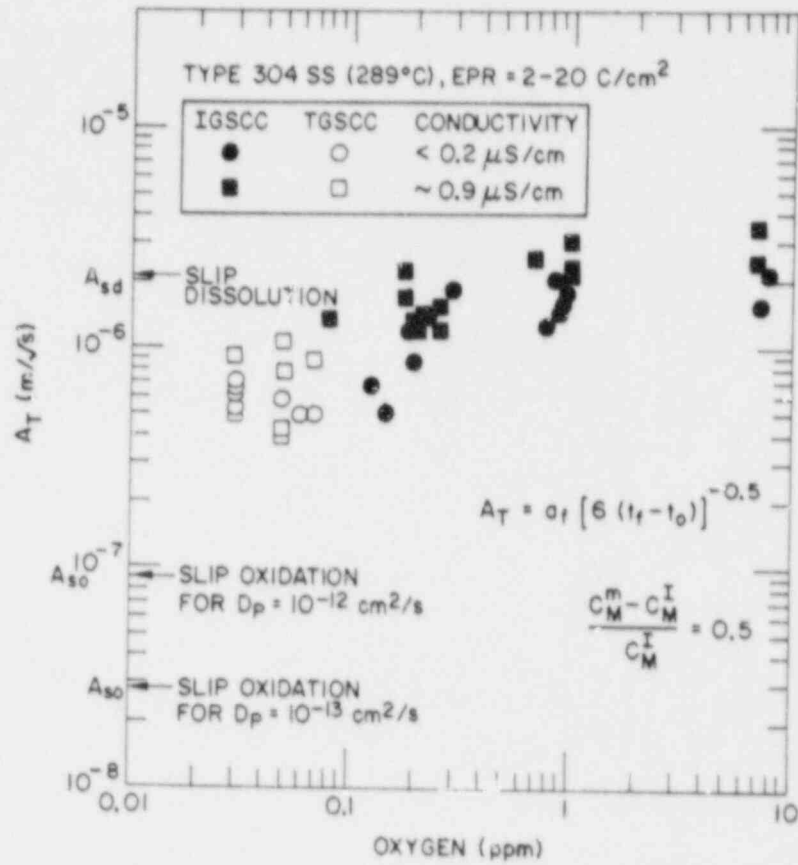
Fig. 9. Comparison of the Predictions of Slip-Oxidation and Slip-Dissolution Models with Experimental Results.

and analysis suggest that for conditions where IGSCC is the expected mode of cracking, slip-dissolution is the primary mechanism of cracking in normal BWR-type water chemistries. Further interpretation of CERT results to obtain a better understanding of SCC in both conventional and alternative materials is in progress.

        c.   <u>Metallurgical and Residual Sress Studies on Stainless Steel Weldments</u>

Metallographic and residual stress studies are in progress on pipe weldments prepared by several procedures used in the repair and replacement of nuclear reactor piping systems. The metallographic evaluations are being conducted both before and after the weldments have been subjected to residual stress improvement treatments such as MSIP.

        (i)   Metallurgical Examination of Modified Type 347 SS Weldments (J. Y. Park and W. J. Shack)

Metallographic and scanning electron microscopy (SEM) examinations were performed on defects observed at the weld fusion line of a 10-in.-diam weldment (weld W2) obtained from the New York Power Authority. The weldment was fabricated by the insert ring procedure developed at the EPRI NDE Center. Four defects, cracks ~1 to 9 mm in length, were found at the fusion line in the portion (~3/4) of the weldment that was available for examination. The other portion was used for residual stress measurements. Cross sections and SEM photos of the longest defect are shown in Figs. 10 - 12. In the cross section in Fig. 10, the defect is about 76 μm deep. Results of the examination of a weld produced by the German narrow-gap weld process were presented in a previous report.[20] Fewer crack indications were found in this weld than in the narrow-gap weld fabricated without an insert (weld K2), but the available data are not sufficient to conclude that one procedure produces fewer flaws of this type than the other.

EDAX examination indicated that a second phase is present on the faces of this crack. The phase is rich in manganese, silicon, calcium, and sulfur, although some of these elements may be artifacts introduced by the
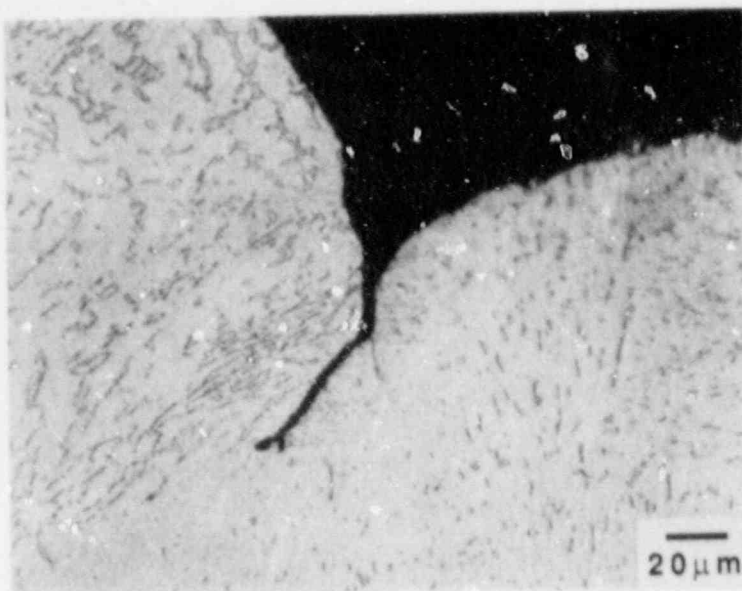
Fig. 10. Cross Section of a Crack in the Weld Fusion Line of a
10-in.-diam Modified Type 347 SS Pipe Weldment at 433X
Magnification.

Fig. 11. Cross Section of Weld Showing the Crack and the
Metallurgical Changes in the Heat-Affected Zone.
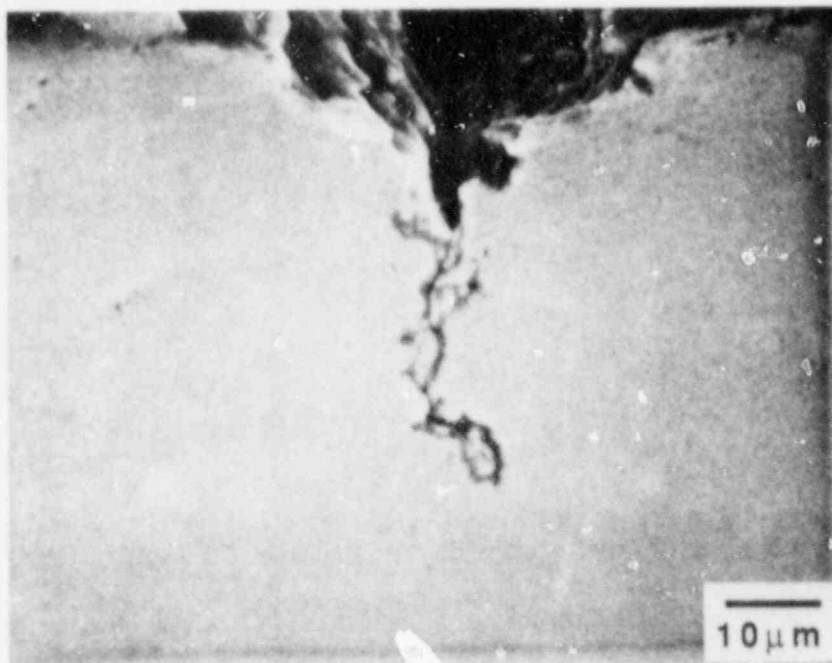
Fig. 12.   SEM Photograph of the Crack Showing a Second Phase
in the Vicinity of the Crack.

dye penetrant.   However, manganese content suggests that actual precipitates
are present.   If a similar phase was associated with the cracks in the narrow-
gap weldment, it was much less obvious.

As part of our work on the MSIP, we have carefully
investigated for flaws of any sort in the weld areas of pipes that have
received an MSIP treatment.   None of the types of flaws that we have observed
in the modified Type 347 SS weldments were observed in our examination of 28-
and 12-in.-diam Type 304/308 SS weldments.   Examination of a small segment
(6-in. long) of a Type 316NG SS weldment revealed no flaws of this nature, but
the piece was too small to be considered representative.   However, on the
basis of the experience of the staff of the EPRI NDE Center, we have concluded
that these flaws can be attributed to improper welding and are not necessarily
characteristic of the modified Type 347 SS.[21]

(ii) Finite Element Analysis of Weldments after MSIP
(E. F. Rybicki, ProSig, Inc.; R. B. Stonesifer,
Computational Mechanics; and W. J. Shack)

Finite element analyses on weldments treated by MSIP were
performed under a subcontract to ProSig, Inc., to study the sensitivity of the
stresses and strains in the pipe wall to variations in the material properties
and the applied compressive strains imposed during MSIP. Since it is
difficult to model precisely the interactions between the MSIP tool and the
weldment (these interactions are also strongly dependent on the details of
the tool design, which are proprietary), two simplified models that represent
bounding solutions were used to perform the analyses in order to determine the
sensitivity of the results to the assumptions in the analysis.

All the calculations were carried out by using an
axisymmetric finite-element model of a 28-in.-diam Schedule 80 pipe. The
finite element grid and pipe geometry are shown in Fig. 13. The model
contains 498 isoparametric four-node elements and 568 nodes. The tool was
assumed to compress a 6-in. axial segment of the pipe. The remote end of the
pipe in the model was not allowed to rotate, but it could move freely in the
axial direction. Since the plastic strains associated with the MSIP
procedure, in general, overwhelm any prior stress state, the pipe was taken to
be stress free at the start of the procedure. The solution was then symmetric
about the mid-plane of the tool.

The calculations were performed with the WELDS finite-
element program.[22] A bilinear elastic-plastic behavior with a kinematic
hardening material model, shown in Fig. 14, was used for the analyses. Since
the plastic strains considered in this study were less than 5%, the bilinear
representation was considered to be adequate. The pipe was also assumed to be
homogeneous; i.e., no allowance was made for the differences in mechanical
properties to be expected in the region of the weld and heat-affected zones
(HAZs). The weld region was simply taken to be the region an appropriate
distance from the tool (~4-6 in. from the pressure band centerline for these
calculations).
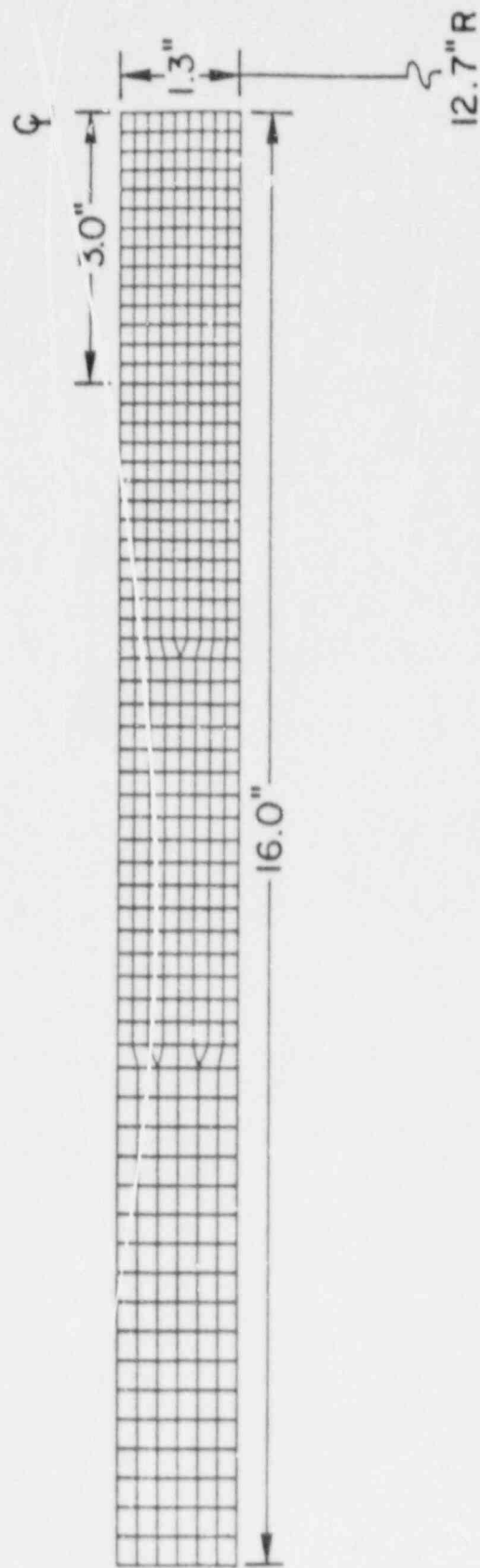
Fig. 13. Axisymmetric Finite Element Grid Used to Model MSIP. The deformations are assumed to be symmetric about the centerline of the tool, which acts over a 6-in.-wide area.
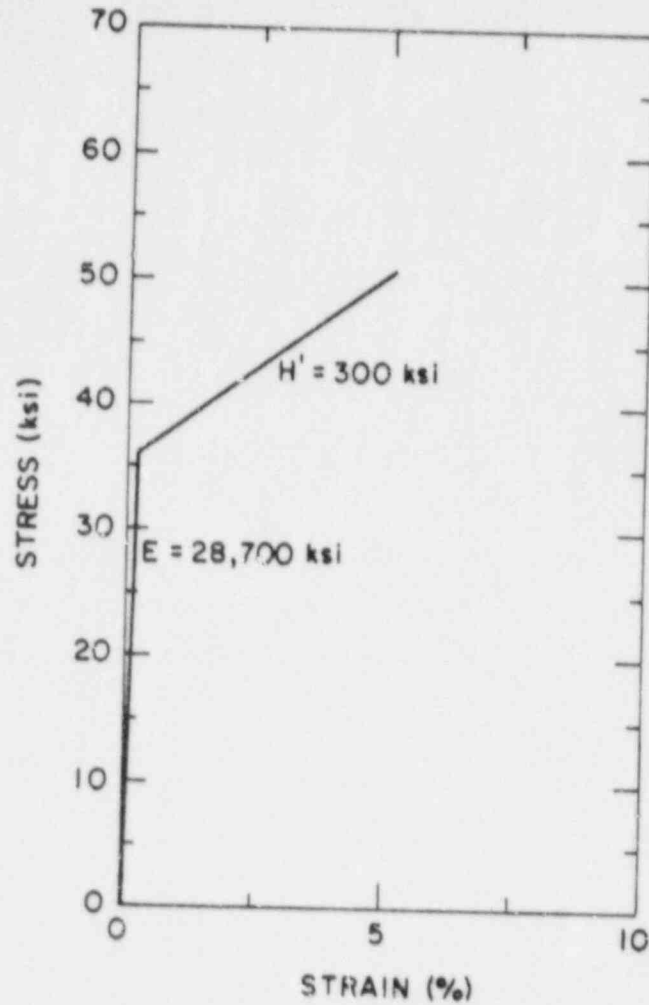
Fig. 14. Stress-Strain Curve for Type 304 SS at Room Temperature.
The initial yield stress is 36 ksi.

Six levels of radial hoop strain (compression) of the
pipe were considered: 1.0, 1.2, 1.4, 1.6, 1.8, and 2.0 percent. Additional
analyses were performed to assess the sensitivity of the results to the
assumed yield stress of the pipe material. The contact pressure distribution
between the tool and the pipe was modeled in terms of two bounding
approximations. In the first model, the pressure between the tool and pipe
surface was assumed to be uniform over the entire contact region. The applied
strain in this case varied with axial position; the average strain was matched
to the applied strain in the MSIP procedure. In the second model, the
displacements produced by the tool were assumed to be uniform.

The inner-surface axial and hoop stresses for an applied hoop strain of 1.6% are shown in Fig. 15. Although the two contact pressure distribution models produced large differences in the stress distributions in the vicinity of the tool, both models gave similar stress distributions in regions more than 1-2 in. from the edge of the tool, which would correspond to the area of interest in an actual weld. The corresponding strain distributions are shown in Fig. 16 and are similar in character. Since the actual loading conditions should be intermediate to these two limiting cases, this finding suggests that the stresses and strains near the weld are not sensitive to the detailed modeling of the tool-pipe interactions. Near the tool the differences are much larger, of course.

Figure 15 also shows experimental measurements of residual stresses on a pipe-to-pipe, 28-in.-diam weldment treated by MSIP.[23] The measurements were made at three azimuths. The data in the figure represent the average values and the ranges of values for the three azimuths at a given axial position. The agreement between the calculated and measured values is reasonably good for the axial stresses, but less satisfactory for the hoop stresses, especially in the region close to the weld, where the magnitudes of the calculated stresses are about half the measured values. The finite-element calculations were not intended to precisely model this particular experiment, and no attempt was made to model the detailed geometry of the weld region. However, the largest source of error may be the high local yield stresses in the weld and HAZs produced by the thermo-mechanical deformations associated with welding.[24] The residual stresses produced by MSIP are strongly dependent on the yield stress of the material. Instead of the nominal 36 ksi yield stress assumed in the analysis, the actual yield stress in the weld material may be closer to 50 ksi.[24]

A comparison of the predicted stresses with a second set of experimental measurements[25] is shown in Fig. 17. These measurements were made on a 28-in.-diam pipe-to-elbow weldment. Although this geometry differs significantly from the geometry assumed in the analysis and from the geometry of the test weldment in Reference 23, there is fairly good agreement between the two sets of measured axial stresses. The agreement between the two sets of measured hoop stresses is less satisfactory; they are fairly close near to

Fig. 15.   Axial and Hoop Stresses on the Inner Surface for Deformation by a
Uniform Pressure or a Uniform Displacement Over the Tool Area.
Experimental data from Reference 23 are shown for comparison.

Fig. 16.   Equivalent Plastic Strain Distributions on the Inner Surface
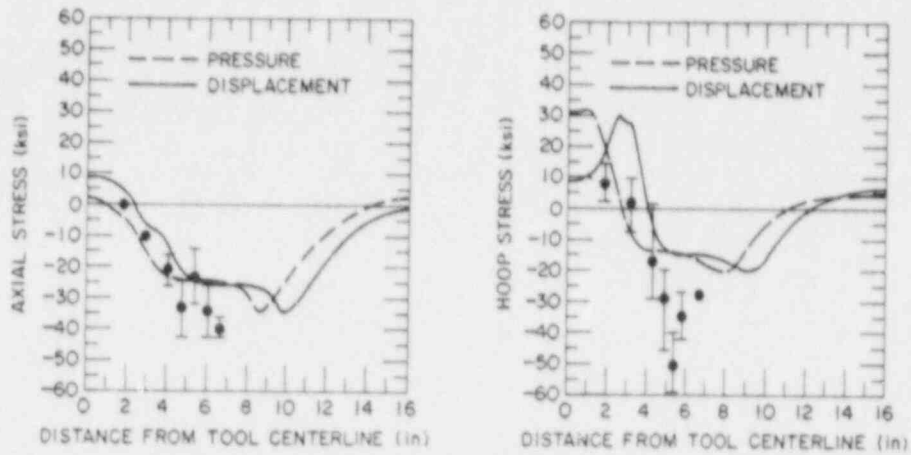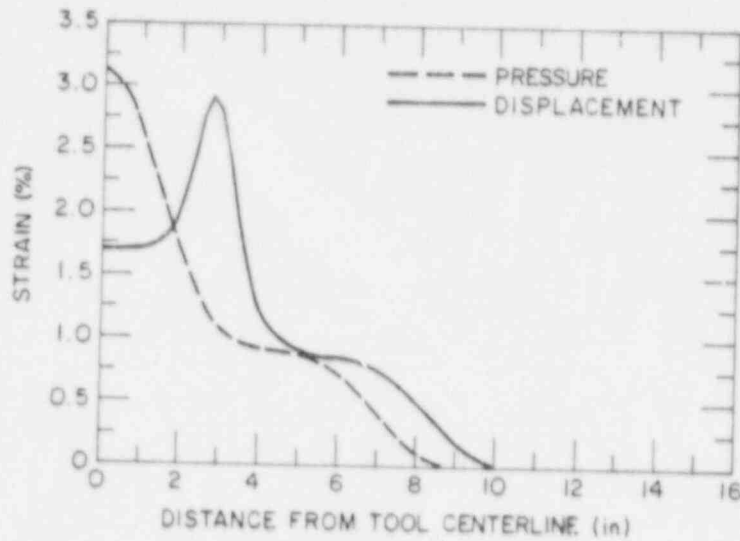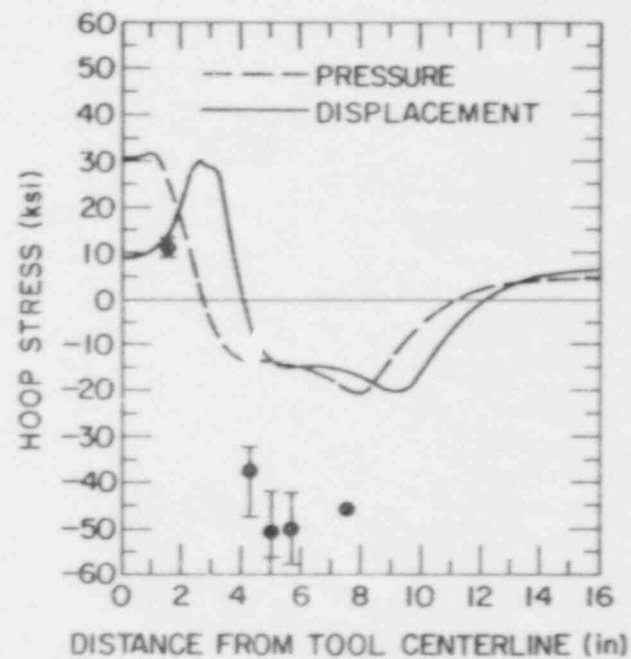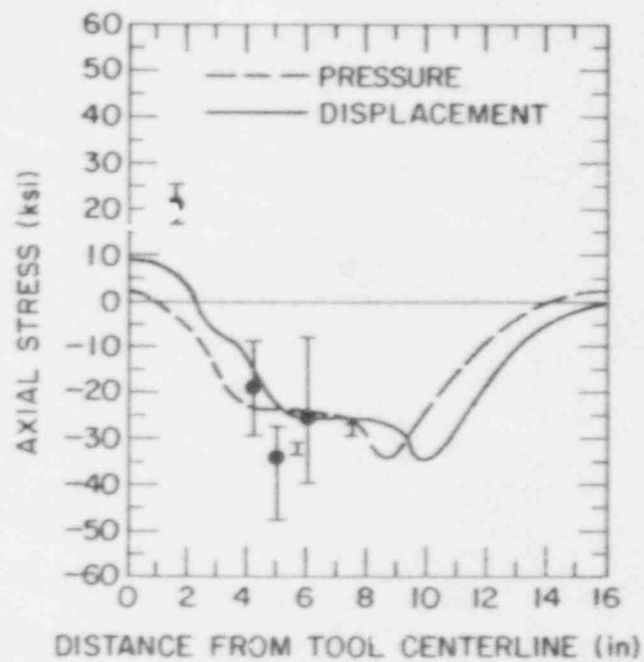for an Applied Strain of 1.6%.

Fig. 17. Axial and Hoop Stresses on the Inner Surface for Deformation by a Uniform Pressure or a Uniform Displacement Over the Tool Area. Experimental data from Reference 25 are shown for comparison.

the weld, but the measurements in Reference 23 show a steeper axial gradient than those in Reference 25. With such substantial differences in geometry, significant differences are not unexpected. Because a wider tool was used for this experiment than for the analysis, the experimental data points have been shifted axially to maintain the same relative position with respect to the edge of the tool. Again, the agreement between the calculated results and the measurements is reasonably good for the axial stresses, but the calculation under predicts the magnitude of the hoop stresses. In Reference 25, residual stress measurements were made prior to MSIP. The measured axial residual stresses were 40-60 ksi, which again indicates that the actual yield stress in the weld and HAZ region is much higher than the 36 ksi appropriate for the base metal. The model also over-predicts the final displacement under the tool (~250 mils compared to the measured ~175 mils); this discrepancy is probably due to differences in elastic springback during unloading associated with the substantial differences in geometry between the model and the experiment.

Axial and hoop residual stress distributions on the inner surface are shown in Fig. 18 for nominal applied strains of 1.0, 1.2, 1.4, 1.6, 1.8, and 2.0%. The residual stresses are insensitive to the level of the applied strain. The equivalent plastic strains on the inner surface of the pipe as a function of the applied strain are shown in Fig. 19. The plastic strains show substantially more variation with applied strain than do the stresses. For applied hoop strains below a certain threshold strain value, the final MSIP residual stresses will depend on the applied strain level and the initial residual stress state. Above this threshold level, the MSIP stresses near the weld are insensitive to the applied strain (Fig. 18). However, the results in Fig. 19 suggest that, in the region under the tool, the strain levels on the inner surface would increase rapidly with the applied strains, although the details of the strain distributions would be sensitive to the design of the tool and the nature of the tool-pipe interactions. The threshold value of the applied strain cannot be determined from the present results, but the computed plastic strain levels suggest that at or above 1.5% the strains are large enough to overwhelm any preexisitng stresses.
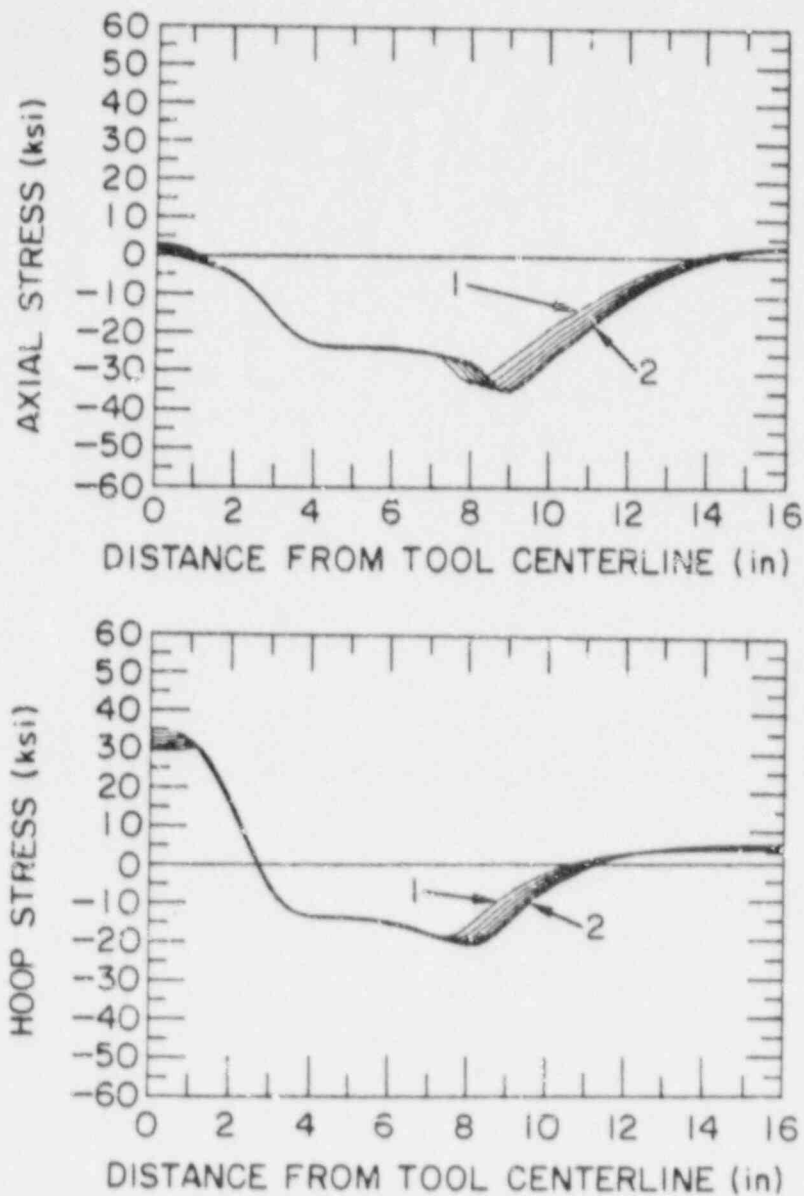
Fig. 18. Residual Stress Distributions on the Inner Surface for Nominal Applied Strains of 1.0, 1.2, 1.4, 1.6, 1.8, and 2.0%. The stresses were calculated by using the uniform pressure model.
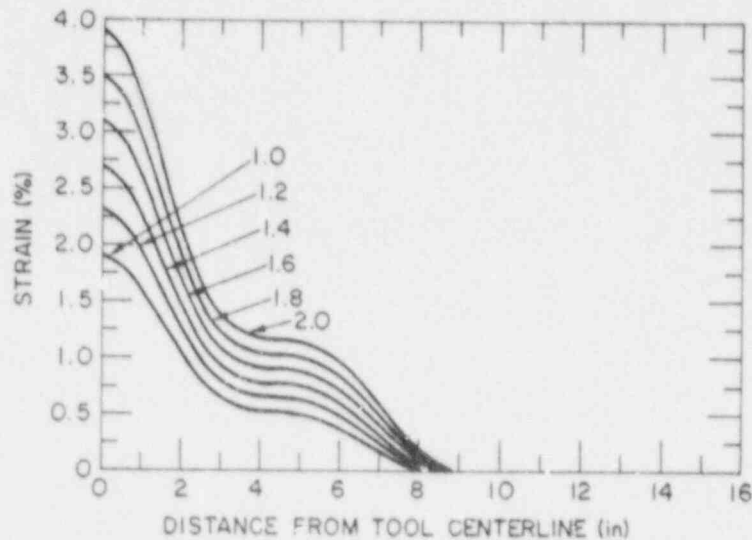
Fig. 19. Equivalent Plastic Strains on the Inner Surface for Nominal Applied Strains of 1.0, 1.2, 1.4, 1.6, 1.8, and 2.0%. The strains were calculated by using the uniform pressure model.

The dependence of the residual stresses on the yield stress of the material is illustrated in Fig. 20. The magnitude of the stresses appears to vary proportionately with the yield stress, as is expected.

B. Influence of Water Chemistry on SCC of Sensitized Type 304 SS
(W. E. Ruther, W. K. Soppet, and T. F. Kassner)

1. Introduction

The objective of this work is to evaluate the potential effectiveness of proposed actions to solve or mitigate the problem of IGSCC in BWR systems through modifications of water chemistry. In this regard, the synergistic effects of dissolved oxygen (produced by radiolytic decomposition of the water) and impurities (e.g., oxyacids from decomposition of ion exchange resins during intrusions into the primary system) on the IGSCC susceptibility and crack growth properties of austenitic stainless steels have been evaluated. The potential benefits associated with small additions of
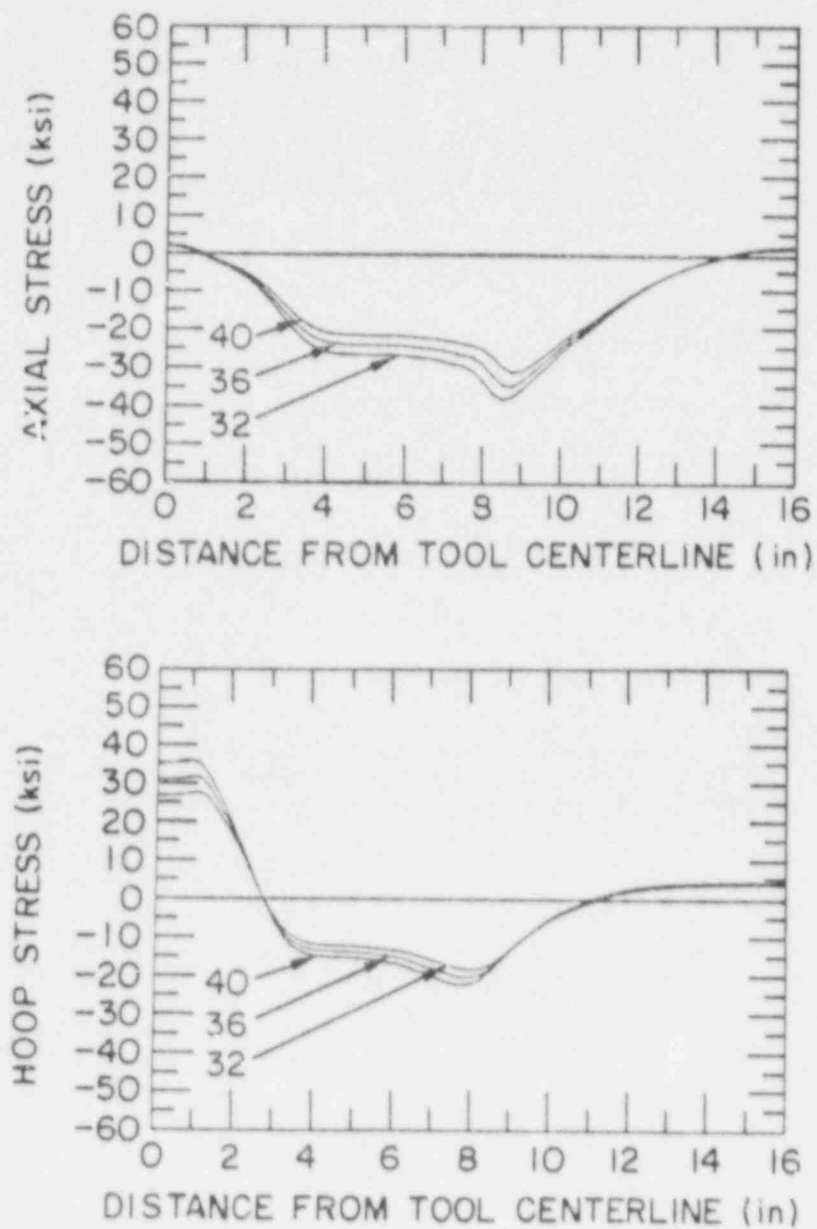
Fig. 20.   Predicted Inner Surface Stresses as a Function of Yield
Stress of the Material after Application of the MSIP
(1.6% Applied Hoop Strain).

hydrogen to the coolant were also evaluated under conditions in which ionic impurities (viz., oxyanions) were also present at low concentrations in the high-temperature water. The results of this work suggest that SCC of the sensitized steel is controlled by the rate of cathodic reduction of dissolved oxygen and/or the oxyanion impurity species in the high-temperature water.[26,27] The crack growth behavior of the steels was correlated with the type and concentration of impurities in the water as well as the open-circuit corrosion potential of the steel. The influence of metallic and organic impurities on SCC of sensitized stainless steel is presently being investigated.

2. **Technical Progress**

a. **Effect of Cupric Ion in Low-Oxygen Water on SCC**

Along with various ionic species that can enter BWR coolant water from leaks in condenser tubes and from the condensate polishing system itself, including resin fines, metallic impurities (corrosion products) from the feedwater train are also transported in the reactor water. In addition to soluble and insoluble iron, copper is also present in the water in plants with admirality brass, aluminum brass, or copper-nickel condenser tubes and/or copper alloy feedwater heaters. The copper concentration in BWR water is of primary concern from the standpoint of deposition on the Zircaloy fuel cladding, which can lead to crud-induced localized corrosion (CILC) and fuel element failures at relatively low burnup.[28,29] The CILC failures occurred primarily in $(U.Gd)O_2$ fuel rods in BWRs with admiralty brass condensers and filter-demineralizer condensate water cleanup systems, which are not as effective as deep resin beds for removal of copper from the water.[29] Copper corrosion products are also present in secondary-system water of pressurized water reactors (PWRs) and can lead to pitting of steam generator tubes[30,31] and contribute to accelerated corrosion of carbon steel tube support plates.[32,33] The effect of copper species at low concentrations on the SCC of reactor materials has not been studied as extensively as that of other impurity species. However, cupric ion at relatively high concentrations (~20 to 90 ppm) in oxygenated (0.2 ppm O_2) water at 250°C enhances IGSCC of sensitized Type 304 SS.[34]

During this reporting period, the effect of cupric chloride on the SCC susceptibility of sensitized Type 304 SS was investigated in water at a low dissolved-oxygen concentration at 150, 200, and 289°C. Cu^{2+} is capable of undergoing cathodic reduction in high-temperature water, and thus could contribute to SCC by providing a cathodic-reduction partial process that couples with the anodic dissolution at the crack tip in a slip-dissolution mechanism[35,36] for crack growth. The CERT experiments were performed in low-oxygen (<5 ppb), near-neutral water to minimize the contribution of other species that can also undergo cathodic reduction (viz., O_2, H_3O^+, and SO_4^{2-}). The role of pH in SCC susceptibility at several copper concentrations in the feedwater was also investigated at 289°C.

(i) Influence of Temperature

Previous CERT results[26,27] indicated that the crack growth rate of sensitized Type 304 SS in high-temperature water at very low dissolved-oxygen concentrations (<5 ppb) was largely controlled by the rate of cathodic reduction of oxyanions (e.g., SO_4^{2-}, NO_3^-, PO_4^{3-}, ClO_4^{3-}, AsO_4^{3-}) having a central atom (S, N, P, Cl, or As) that can assume different oxidation states. Subsequently, CERT experiments were performed in 289°C water containing salts with a cation that can undergo reduction in water (e.g., Cu^{2+}) as well as with cations that have a single oxidation state (viz., Zn^{2+}, Mg^{2+}, and Na^+). The latter results indicated that only Cu^{2+} facilitated SCC analogously to dissolved oxygen and the various oxyanions.[37]

Since the cupric ion concentration that caused severe IGSCC in the steel (i.e., >2 ppm) was considerably higher than typical values encountered in the feedwater of BWRs (<0.3 ppb)[38] and in recirculating and once-through steam generators in PWRs (<2 ppb),[39] a series of CERT experiments was performed to determine the minimum concentrations of this species required for cracking at 150 and 200°C as well as at 289°C. As in the previous tests, it is essential to minimize the concentration of other species that can also participate in cathodic reduction partial processes that couple with anodic dissolution at the crack tip and govern crack growth by a slip-dissolution[35] or slip-oxidation[17] mechanism. Consequently, the tests were performed with chloride salts in low-oxygen, near-neutral water ($pH_{25°C}$ > 5.7) to

specifically minimize the contributions from the reduction of O_2, H_3O^+, and oxyanions of various salts (viz., SO_4^{2-}). As in previous work, the open-circuit corrosion potential (ECP) of Type 304 SS and the redox potential of platinum were determined versus an external 0.1M KCl/AgCl/Ag reference electrode, and the values were converted to the standard hydrogen electrode. A copper electrode was also included in the tests performed at 150 and 200°C. In the most recent tests, the effluent water was collected, and the copper concentrations were determined by inductively-coupled-plasma (ICP) spectroscopy analyses.

The feedwater chemistries, CERT parameters, and the ECP results are given in Table 8. The CERT data indicate a marked increase in SCC susceptibility for feedwater Cu^{2+} concentrations above ~1 and 2 ppm at 200 and 289°C, respectively. This is illustrated in Fig. 21 by the dependence of the time to failure on Cu^{2+} concentration and conductivity of the feedwater. The corresponding measured effluent copper concentrations for the transition from either 100% ductile fracture or ~20% TGSCC to ~90-100% IGSCC are ~0.5 and 1 ppm at the respective temperatures. At 150°C, IGSCC occurred for feedwater Cu^{2+} concentrations of > 0.1 to 10.0 ppm, and the crack growth rates increased with Cu^{2+} concentration over this range, as is shown in Fig. 22. On the basis of limited data, the crack growth rate increases with the 1/2 power of the Cu^{2+} concentration, which is consistent with the cathodic-reduction partial process of $Cu^{2+} + 2e^- = Cu°$. At 289°C the crack growth rate is virtually independent of Cu^{2+} concentration over the range of ~3 to 20 ppm. This suggests that the film rupture rate at the crack tip, which depends on the applied strain rate, is dominant over the rate of reduction of Cu^{2+} in determining the magnitude of the crack growth rate at these relatively high concentrations. Visible $Cu°$ deposition was evident on the surfaces of the autoclave, pull rods, and specimens, particularly at higher copper concentrations in the feedwater. Metallic copper particles were identified by electron microprobe analyses of the surfaces of several specimens.

The electrochemical potential values for Type 304 SS indicate that IGSCC does not occur for values below approximately -290 mV(SHE) at 289°C, which is consistent with results obtained with either dissolved oxygen or other impurity species.[19,41] The ECP values for Type 304 SS at 200°C indicate that IGSCC does not occur at values below approximately

Table 8. Influence of Temperature on the SCC Susceptibility of Sensitized Type 304 SS Specimens[a] in Water Containing $CuCl_2$ at a Low (<5 ppb) Dissolved-Oxygen Concentration

Test No.	Temp., °C	Cation Concentration Influent, ppm	Cation Concentration Effluent,[b] ppm	Anion Conc., ppm	Cond. at 25°C, µS/cm	pH at 25°C	Failure Time, h	Maximum Stress, MPa	Total Elong. in, %	Reduction in Area, %	Fracture Morphology[c]	SCC Growth Rate,[d] m s^{-1}	Type 304 SS, mV(SHE)	Pt, mV(SHE)	Cu, mV(SHE)
194	289	-	-	-	0.08	6.48	154	535	55	57	0.81D, 0.19T	8.3 x 10^{-10}	-491	-430	-
183	289	0.5	-	0.56	2.4	5.98	152	545	55	66	1.00D	-	-290	-283	-
179	289	2.0	-	2.23	9.4	5.57	155	536	56	70	1.00D	-	-315	-282	-
190	289	3.0	0.95	3.33	13.5	5.78	27	240	10	13	0.08D, 0.92G$_3$	5.8 x 10^{-8}	-27	-216	-
201	289	3.0	1.71	3.33	12.8	5.84	25	256	9	13	0.06D, 0.54G$_3$	5.4 x 10^{-8}	-285	-239	-
182	289	5.0	-	5.58	22.0	5.56	27	245	10	12	0.08D, 0.92I	6.2 x 10^{-8}	135	-63	-
181	289	10.0	-	11.21	42.0	5.58	34	292	12	12	0.16D, 0.84I	2.2 x 10^{-8}	-50	-72	-
180	289	20.0	-	22.40	83.5	5.57	37	3C1	13	12	0.10D, 0.90I	2.4 x 10^{-8}	-181	-82	-
203	200	0.2	0.25	0.22	1.2	6.06	147	521	53	79	1.00D	-	-141	-152	-127
204	200	1.0	0.41	1.10	4.3	6.02	151	521	54	78	1.00D	-	-91	-96	-90
206	200	2.0	1.03	2.20	8.4	5.89	15	235	5	15	0.01D, 0.99I	8.9 x 10^{-8}	234	181	-83
205	200	5.0	2.56	5.50	20.0	5.81	13	128	5	9	1.00I	9.1 x 10^{-8}	168	-67	-19
221	150	0.1	0.12	0.11	0.67	6.25	156	527	56	81	1.00D	-	228	-71	-23
210	150	0.25	0.19	0.27	1.3	6.00	102	493	37	68	0.33D, 0.68G$_3$	6.4 x 10^{-9}	244	243	-38
209	150	0.5	0.45	0.55	2.3	5.98	67	421	24	34	0.47D, 0.53I	1.1 x 10^{-8}	256	254	-23
207	150	1.0	0.72	1.10	4.3	5.99	65	416	23	47	0.45D, 0.55I	1.4 x 10^{-8}	282	280	5
208	150	2.0	1.49	2.20	8.4	5.88	53	359	19	52	0.31D, 0.69G$_3$	1.9 x 10^{-8}	282	277	17
225	150	5.0	3.56	5.50	20.5	5.87	44	315	16	24	0.21D, 0.79I	2.5 x 10^{-8}	239	231	19
224	150	10.0	6.91	11.00	41.0	5.75	26	251	9	20	0.06D, 0.94I	4.0 x 10^{-8}	262	253	51

[a]Lightly sensitized (EPR = 2 C/cm^2) specimens (Heat No. 30956) were exposed to the environments for ~20 h before being strained at a rate of 1 x 10^{-6} s^{-1}

[b]Copper concentration of the effluent water was determined by ICP spectroscopy analyses.

[c]Ductile (D), transgranular (T), granulated (G), and intergranular (I), in terms of the fraction of the cross-sectional area. Characterization of the fracture surface morphologies is in accordance with the illustrations and definitions in Reference 40.

[d]SCC growth rates are based on measurement of the depth of the longest crack in an enlarged micrograph of the fracture surface and the time period from the onset of yield to the point of maximum load on the tensile curve.

(a)

TIME TO FAILURE (h)

160
140
120
100
80
60
40
20
0

0.01 0.1 1 10

Cu^{2+} (ppm)

TEMPERATURE
□ 289°C
△ 289°C
○ 200°C

SENSITIZATION
EPR = 2 C/cm²

STRAIN RATE
$\dot{\epsilon} = 1\times10^{-6} s^{-1}$

FRACTURE MODE
OPEN = D + TG
CLOSED = D + IG

(b)

TIME TO FAILURE (h)

160
140
120
100
80
60
40
20
0

0.1 1 10 100 200

CONDUCTIVITY at 25°C (µS/cm)

TEMPERATURE
□ 289°C
△ 289°C
○ 200°C

SENSITIZATION
EPR = 2 C/cm²

STRAIN RATE
$\dot{\epsilon} = 1\times10^{-6} s^{-1}$

FRACTURE MODE
OPEN = D + TG
CLOSED = D + IG

Fig. 21. Dependence of Time to Failure of Lightly Sensitized
(EPR = 2 C/cm²) Type 304 SS Specimens on (a) Cupric Ion
Concentration and (b) Conductivity of the Low Oxygen
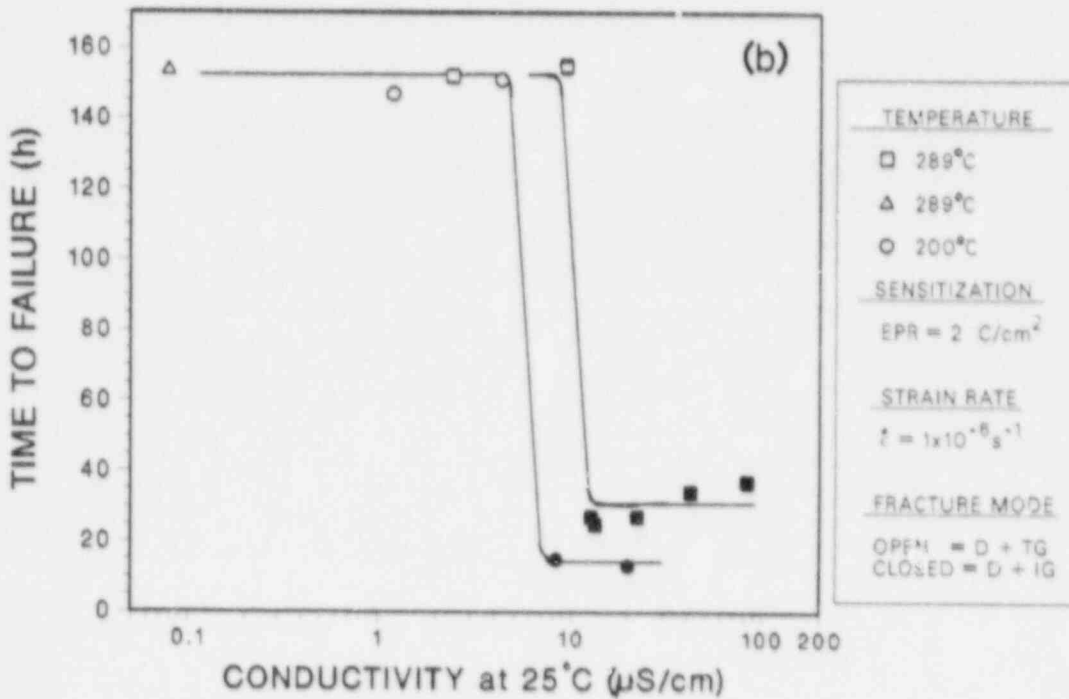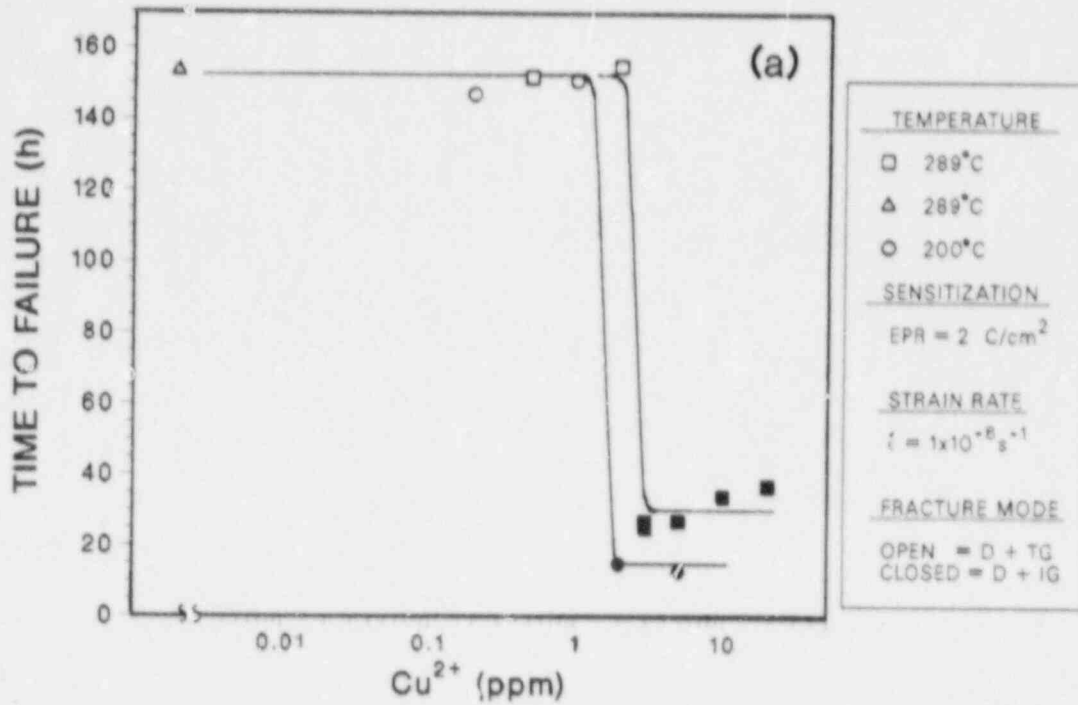(<5 ppb) Feedwater in CERT Experiments at 200 and 289°C.
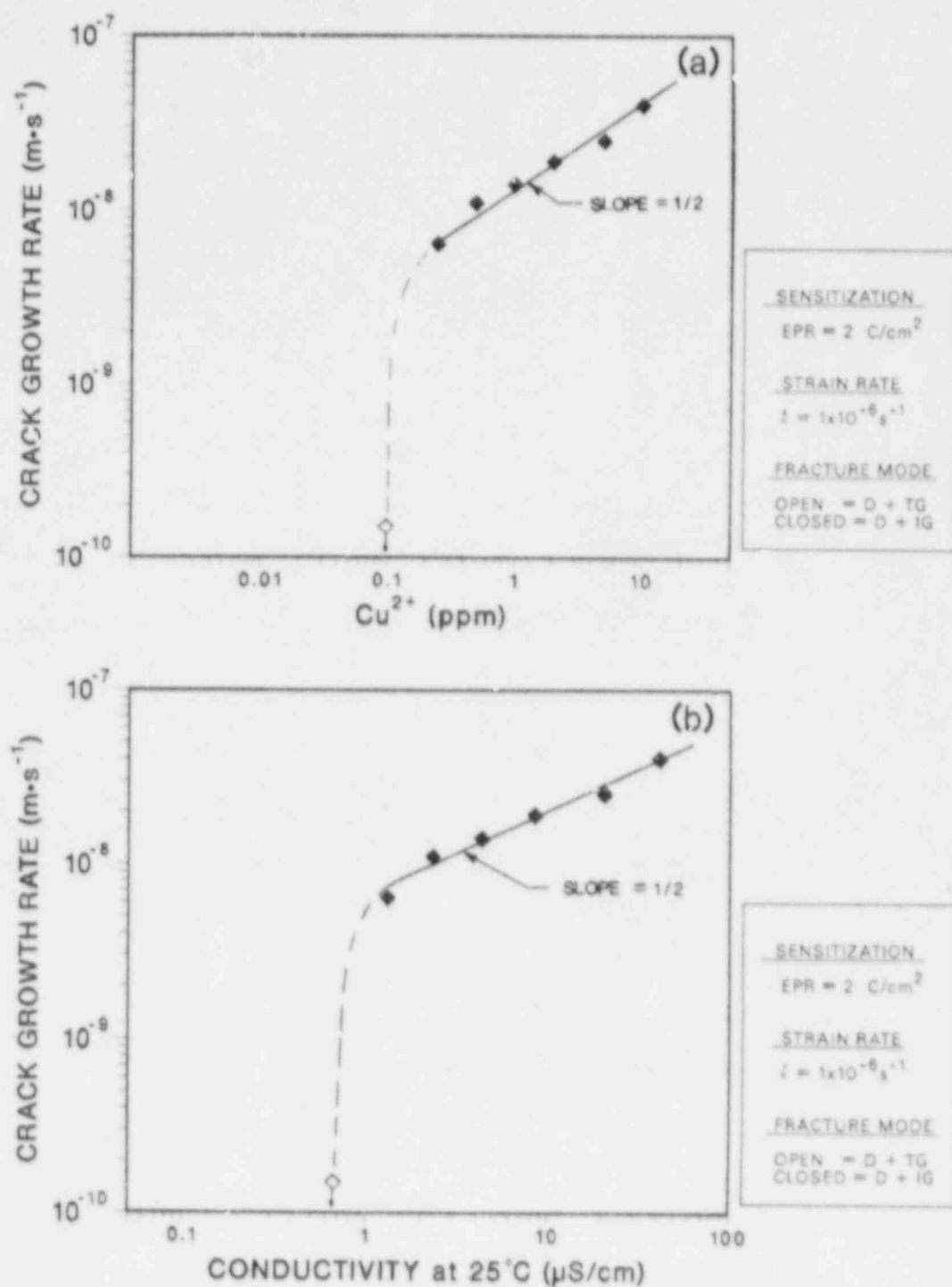
42

Fig. 22. Dependence of the Crack Growth Rate of Lightly Sensitized
(EPR = 2 C/cm²) Type 304 SS Specimens on (a) Cupric Ion
Concentration and (b) Conductivity of the Low-Oxygen
(<5 ppb) Feedwater in CERT Experiments at 150°C.

-90 mV(SHE), and the corresponding value at 150°C is approximately
230 mV(SHE). For a given water chemistry, the ECP of the steel and platinum
increase as the temperature decreases. The dependence of the ECP of the steel
and platinum on temperature for Cu^{2+} concentrations of 1-2 ppm is shown in
Fig. 23. The curves are similar to those in Fig. 24, reported previously[42,43]
for high-purity water with 0.2 ppm dissolved oxygen and 0.1 and 1.0 ppm
sulfate as H_2SO_4 at this oxygen level.

(ii) Influence of pH of Several Cu^{2+} Solutions at 289°C

Several CERT tests were performed at 289°C to explore the
effect of pH on the SCC behavior of sensitized Type 304 SS at Cu^{2+}
concentrations of 1, 3, and 5 ppm in the low-oxygen feedwater. Although the
results in Table 9 are not extensive, the data reveal the following trends.
For a cupric ion concentration below the value that results in IGSCC in the
low-oxygen water (e.g., 1 ppm), a higher pH (~8.7 versus 5.9 at 25°C) produced
by adding morpholine to the feedwater had no effect on the SCC behavior; i.e.,
CERT parameters were essentially the same for the two conditions. At a Cu^{2+}
concentration of 3 ppm, severe IGSCC occurred at $pH_{25°C}$ ~ 5.8; however,
additions of either morpholine ($pH_{25°C}$ of ~6.7 to 8.5) or HCl ($pH_{25°C}$ of ~3.7
to 4.8) caused a significant decrease in IGSCC susceptibility. At a Cu^{2+}
concentration of 5 ppm, an increase in pH was also beneficial; the mode of
cracking remained intergranular but the rate was significantly lower.

The distinct transition between predominantly ductile
fracture and severe IGSCC over a small concentration range in near-neutral
water and the strong effect of pH on SCC susceptibility at a fixed Cu^{2+}
concentration may be related to the solubility of various copper species (CuO,
Cu_2O, and Cu^+) in the water. Preliminary calculations suggest that IGSCC
occurs when the concentration of cupric ion is higher than the solubility of
Cu_2O or Cu^+ at the test temperature. The dependence of SCC on pH may also be
related to changes in the solubility of these phases. Although the effluent
copper concentrations in Tables 8 and 9 are lower by a factor of ~2 than those
in influent, near-neutral feedwater, the values are lower by a factor of ~100
in the basic solutions. In acid solutions (Table 9), the effluent and
influent copper concentrations are virtually the same. In test No. 199

44
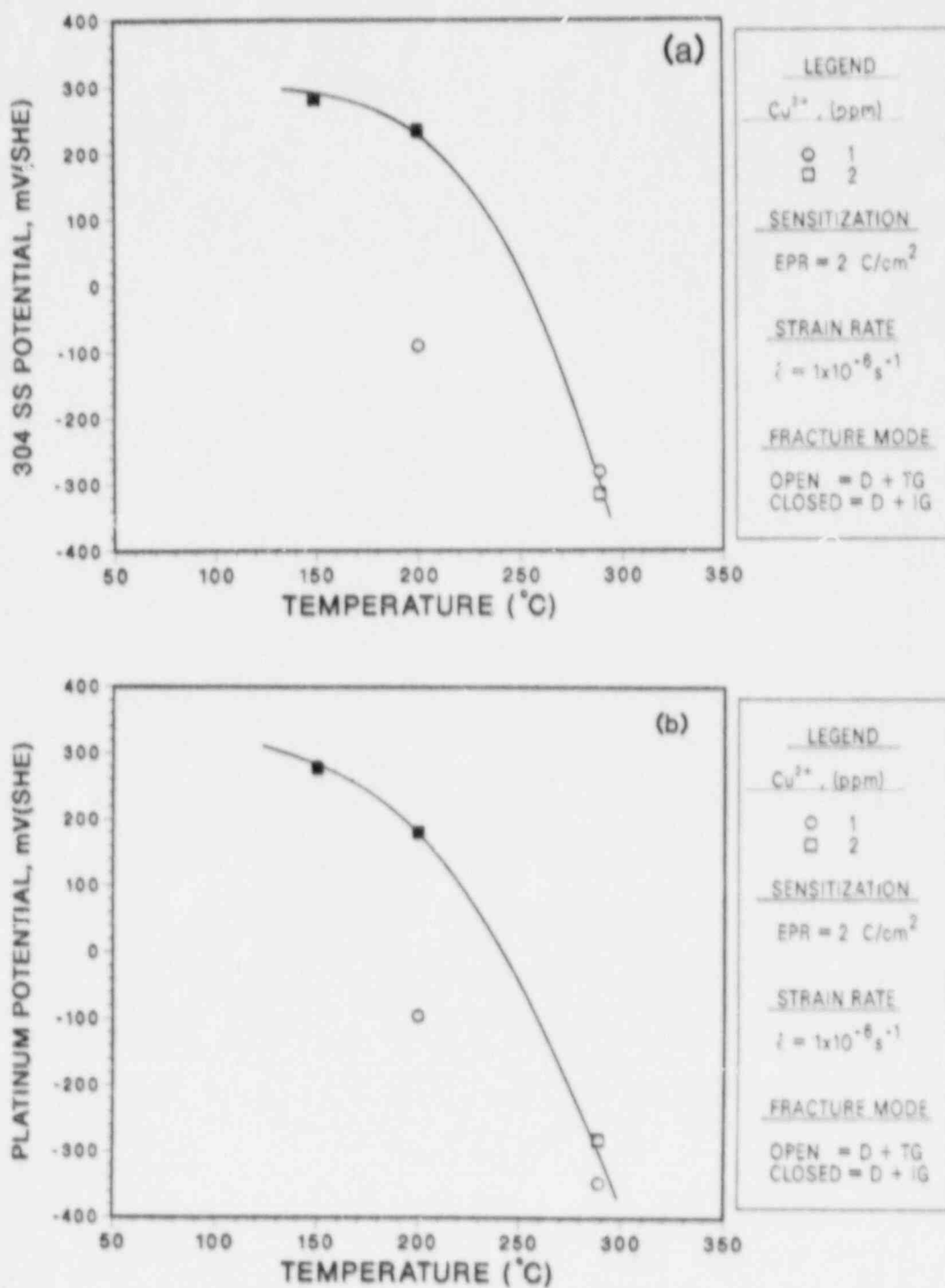
Fig. 33. Dependence of the Steady-State Electrochemical Potential of (a) Type 304 SS and (b) Platinum on Temperature during CERT Experiments on Lightly Sensitized Type 304 SS Specimens in Low-Oxygen (<5 ppb) Water Containing 1-2 ppm Cu^{2+} as $CuCl_2$ or $CuSO_4$.
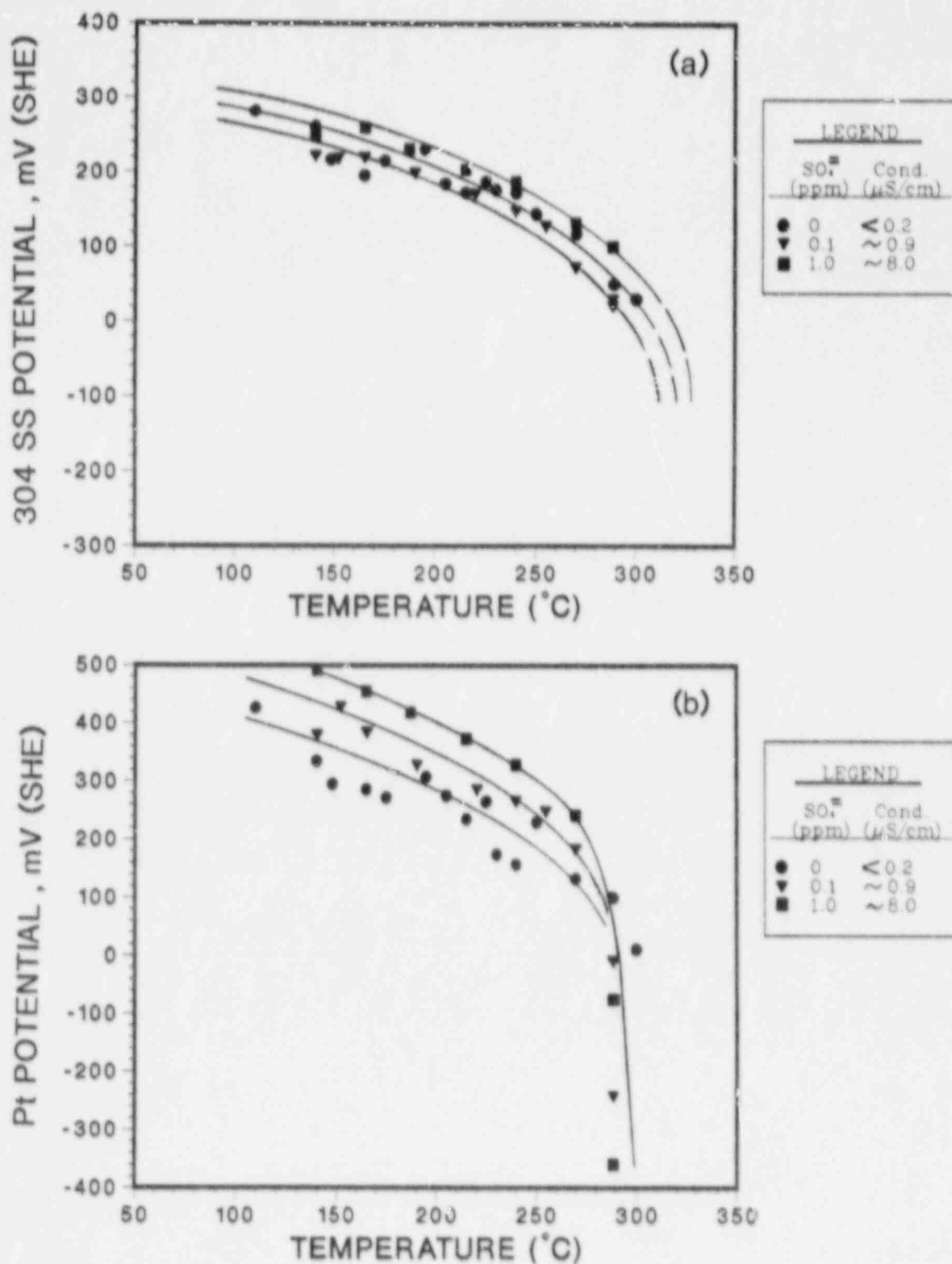
Fig. 24. Effect of Temperature on the Electrochemical Potential of
(a) Type 304 SS and (b) Platinum in Water Containing 0.2 ppm
Dissolved Oxygen and 0, 0.1, and 1.0 ppm Sulfate as H_2SO_4.[42,43]

Table 9. Influence of pH on the SCC Susceptibility of Sensitized Type 304 SS Specimens[a] in Water at 289°C Containing Copper Salts at a Low (<5 ppb) Dissolved Oxygen Concentration

	Feedwater Chemistry							CERT Parameters						Potential	
Test No.	Impurity Species	Cation Concentration Influent, ppm	Cation Concentration Effluent,[b] ppm	Anion Conc., ppm	Cond. at 25°C, µS/cm	pH at 25°C	Failure Time, h	Maximum Stress, MPa	Total Elong., %	Reduction in Area, %	Fracture Morphology[c]	SCC Growth Rate,[d] m s⁻¹	Type 304 SS, mV(SHE)	Pt, mV(SHE)
194	–	–	–	–	0.06	6.48	154	535	55	57	0.81D, 0.19T	8.3×10^{-10}	-491	-430
192	CuSO₄	1.0	0.21	1.54	4.6	5.87	138	533	50	48	0.74D, 0.26T	2.4×10^{-9}	-281	-347
195	CuSO₄	1.0	0.04	1.54	4.2	8.69[e]	149	533	54	57	0.73D, 0.27T	1.7×10^{-9}	-426	-388
199	CuCO₂	3.0	6.63	3.33	125.0	3.65[f]	104	481	37	34	0.45D, 0.55I	5.7×10^{-9}	-357	-348
198	CuCO₂	3.0	2.11	3.33	22.0	4.77[f]	153	540	55	74	1.00D	–	-224	-218
190	CuCO₂	3.0	0.95	3.33	13.5	5.78	27	240	19	13	0.06I, 0.92G₃	5.8×10^{-8}	-27	-216
201	CuCO₂	3.0	1.71	3.33	12.8	5.84	25	256	9	13	0.06I, 0.94G₃	5.4×10^{-8}	-285	-239
200	CuCO₂	3.0	1.88	3.33	12.4	8.58[e]	158	535	57	75	1.00D	–	-274	-233
202	CuCO₂	3.0	0.03	3.33	11.5	7.79[e]	156	529	58	80	3.84D, 0.16T	1.4×10^{-9}	-440	-438
196	CuSO₄	3.0	0.02	4.62	10.3	8.55[e]	125	529	45	46	0.80D, 0.20I	3.0×10^{-9}	-333	-360
182	CuCO₂	5.0	–	5.58	22.0	5.56	27	245	10	12	0.08D, 0.92I	6.2×10^{-8}	135	-63
189	CuSO₄	5.0	–	7.70	22.0	5.73	46	301	17	12	0.12D, 0.88G₃	2.8×10^{-8}	-72	-182
197	CuSO₄	5.0	0.05	7.70	18.0	8.49[e]	100	504	36	47	0.57D, 0.43G₃	6.1×10^{-9}	-304	-325

[a] Lightly sensitized (EPR = 2 C/cm²) specimens (Heat No. 30956) were exposed to the environments for ~20 h before being strained at a rate of 1×10^{-6} s⁻¹.

[b] Copper concentration of the effluent water was determined by ICP spectroscopy analyses.

[c] Ductile (D), transgranular (T), granulated (G), and intergranular (I), in terms of the fraction of the cross-sectional area. Characterization of the fracture surface morphologies is in accordance with the illustrations and definitions in Reference 40.

[d] SCC growth rates are based on measurement of the depth of the longest crack in an enlarged micrograph of the fracture surface and the time period from the onset of yield to the point of maximum load on the tensile curve.

[e] pH adjusted with morpholine.

[f] pH adjusted with HCl.

($\text{pH}_{25°C}$ = 3.65), the effluent copper concentration was actually higher than the feedwater concentration because of dissolution of copper from surfaces of the autoclave and piping under the more acidic condition. A quantitative description of the effects of copper ion concentration, pH, and temperature on SCC susceptibility of Type 304 SS is being developed from analogous experiments with CuCl additions to the low-oxygen feedwater.

b. Effect of Organic Acids on SCC in 289°C Water with 0.2 ppm Dissolved Oxygen

Potential chemical contaminants[44] and possible pathways[45] for entry of various substances into BWR reactor coolant systems have been evaluated. Typical chemicals at power plants include paint products, glycol, hydraulic fluids, lubricants, detergents, chemical cleaners, laundry chemicals, freons, boiler treatment chemicals, diesel fuel, ion exchange resins, and regeneration chemicals. Of the many pathways by which contaminants can enter the primary coolant, the radwaste floor drain sump system was identified as the predominant source of contamination.[44] This system collects uncontrolled water from open leakage and washdown; consequently, the sumps are open to all spills and dumps. The authors[45] pointed out the common misconception that the radwaste system will treat water to remove any impurity and produce condensate-quality effluent. The process equipment is typically designed to remove ionic species by ion exchange, crud by filtration, and nonvolatiles by evaporation residue, but organic substances can pass through the system and not be detected by turbidity or conductivity instrumentation. The treated radwaste water, with undetected impurities, is transferred to the condensate storage tank and then to the reactor via the feedwater system, where filtration and ion exchange do not hinder the progress of dissolved or finely dispersed organic material.[44] Some of the long-lived products that may exist in the reactor water due to organic intrusions are carboxylic acids, alcohols, phenolics, aromatic hydrocarbons, hydrogen halides, sulfuric and sulfonic acids, amines, and other substances.[44]

Organic impurities are also a concern in pressurized-water reactor (PWR) secondary systems in relation to materials performance and because organic acids increase cation conductivity, which complicates secondary water

monitoring and control. A recent survey of inorganic acids, total organic carbon, and inorganic anions in the secondary water cycles of thirteen PWRs indicated that organic acids were responsible for a major fraction of the cation conductivity in many of the plants.[46] Acetic and formic were the most common acids; however, lactic, propionic, and butyric acid were also present in some of the systems. The make-up water was the major source of the organic impurities, some of which were in colloidal, nonionic form.[46] As in the case of BWR water, these contaminants or their decomposition products could influence the performance of system materials (the corrosion or SCC susceptibility).

We have previously we have quantified the deleterious effects of several inorganic acids and sodium salts with 0.2 ppm dissolved oxygen on the SCC susceptibility of sensitized Type 304 SS and other austenitic stainless steels by means of CERT and cyclic loading tests in simulated reactor coolant water at 289°C.[2,47] For comparison with these results, CERT tests were performed on lightly sensitized Type 304 SS specimens in water at 289°C containing ~0.2 ppm dissolved oxygen and several organic acids at an anion concentration of 1.0 ppm. The results in Table 10 indicate that carbonic, carboxylic (acetic, formic, lactic, and oxalic), and short-chain aliphatic (propionic and butyric) acids do not have a deleterious effect on SCC of the steel under simulated normal BWR water chemistry. Acetic and formic acid at a concentration of 1.0 ppm have almost no effect on the CERT parameters compared with values obtained in high-purity water containing ~ 0.2 ppm dissolved oxygen. In contrast to these results, 1.0 ppm of the other species caused a significant increase in the time to failure, maximum stress, and reduction in area of the specimens with a concomitant decrease in the crack growth rates, as shown in Fig. 25. With the exception of the specimen that underwent transgranular cracking in water containing 1.0 ppm propionic acid, all of the other specimens exhibited an intergranular or granulated fracture morphology. A plot of the crack growth rate versus the conductivity (Fig. 26) does not show the typical decrease in the rate as the water quality improves.

The open-circuit corrosion potentials of Type 304 SS in water containing ~0.2 ppm dissolved oxygen and 1.0 ppm of the various acids were not significantly lower than those in high-purity water at this dissolved-oxygen

Table 10. Influence of Several Organic Acids on the SCC Susceptibility of Sensitized Type 304 SS Specimens[a] in 289°C Water at a Dissolved-Oxygen Concentration of ~0.2 ppm

Test No.	Feedwater Chemistry					CERT Parameters						Potentials	
	Oxygen Conc., ppm	Impurity Acids	Anion Conc., ppm	Cond. at 25°C, μS/cm	pH at 25°C	Failure Time, h	Maximum Stress, MPa	Total Elong., %	Reduction in Area, %	Fracture Morphology[b]	SCC Growth Rate,[c] m·s⁻¹	Type 304 SS mV(SHE)	Pt. mV(SHE)
A144	0.25	–	–	0.26	6.43	73	297	14	15	0.16D, 0.84I	1.5×10^{-8}	98	158
A143	0.18	–	–	0.16	6.21	101	350	19	12	0.16D, 0.84I	9.6×10^{-9}	86	196
A146	0.21	Acetic	1.0	3.9	5.07	104	390	19	26	0.29D, 0.71I	7.0×10^{-9}	103	111
A147	0.23	Formic	1.0	7.2	4.81	118	393	22	28	0.33D, 0.67I	6.4×10^{-9}	9	-333
A148	0.23	Lactic	1.0	3.7	5.09	161	442	30	36	0.18D, 0.82G	4.3×10^{-9}	-206	-406
A151	0.24	Oxalic	1.0	7.4	4.80	208	513	39	44	0.48D, 0.52G	3.5×10^{-9}	-2	-255
A149	0.25	Proprionic	1.0	3.1	5.16	201	513	38	<1	0.61D, 0.39T	2.9×10^{-9}	26	-134
A150	0.24	Butyric	1.0	2.7	5.27	189	485	35	59	0.83D, 0.17G	2.3×10^{-9}	55	-228
A152	0.22	Carbonic	1.0	0.60	5.90	207	505	39	58	0.79D, 0.21G	2.0×10^{-9}	18	-165

[a] Lightly sensitized (EPR ~ 2 C/cm²) specimens (Heat No. 30956) were exposed to the environments for ~20 h before being strained at a rate of 5.2×10^{-7} s⁻¹.

[b] Ductile (D), transgranular (T), granulated (G), and intergranular (I), in terms of the fraction of the cross-sectional area. Characterization of the fracture surface morphologies is in accordance with the illustrations and definitions in Reference 40.

[c] SCC growth rates are based on measurement of the depth of the longest crack in an enlarged micrograph of the fracture surface and the time period from the onset of yield to the point of maximum load on the tensile curve.
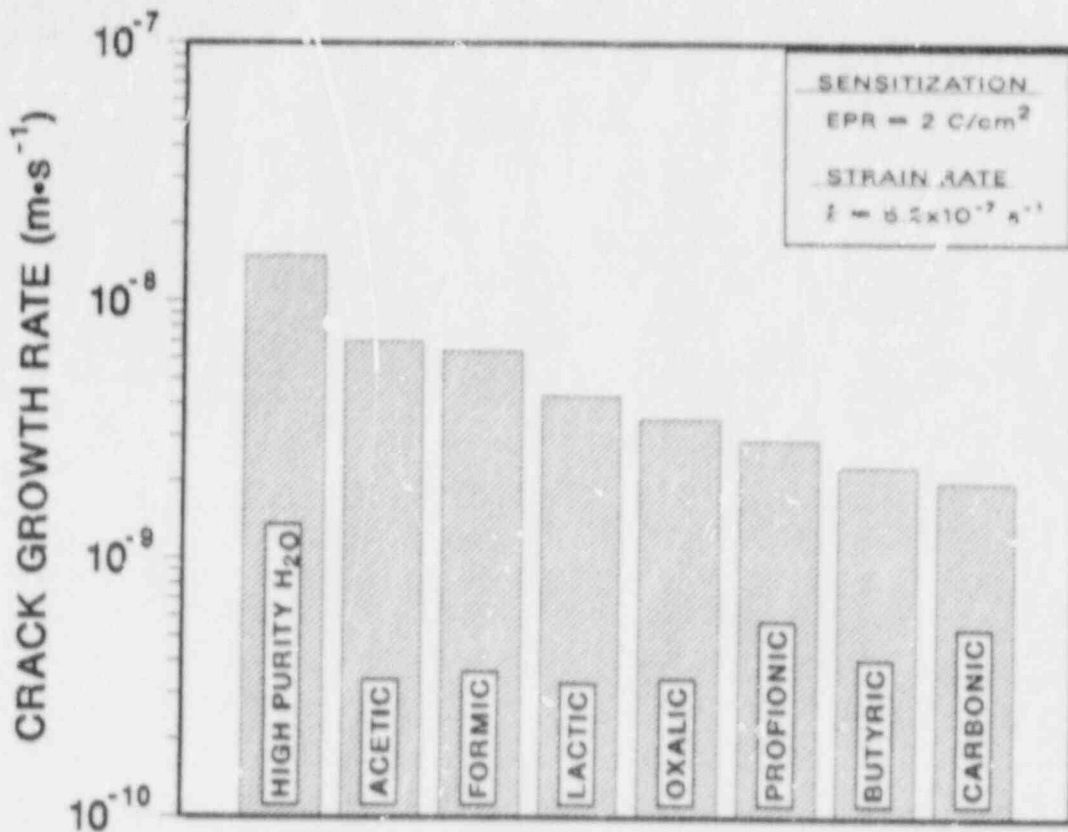
Fig. 25. Effect of Several Carboxylic and Aliphatic Acids at an Anion Concentration of 1.0 ppm in Water Containing 0.2 ppm Dissolved Oxygen on the Crack Growth Rates of Lightly Sensitized Type 304 SS Specimens in CERT Experiments at 289°C and a Strain Rate of 5.2 x 10^{-7} s^{-1}.

concentration, with the exception of the test in water containing 1.0 ppm lactic acid. However, the redox (platinum) potentials in water containing oxygen and the various acids (except for acetic) were considerably more negative than those of stainless steel. Several factors must be considered in order to rationalize the effect of organic acids on SCC susceptibility and the ECP values of Type 304 SS and platinum. For example, organic substances react with dissolved oxygen in high-temperature water. This occurs infrequently in our laboratory testing facilities when a minute crack or pinhole develops in the diaphragm of the positive-displacement feedwater pump, and a small amount of oil is injected into the feedwater during each stroke. This situation manifests itself in considerable oxygen depletion in the effluent water and a concomitantly large decrease in the ECP values to <-450 aV(SHE). During the present tests, the effluent dissolved-oxygen concentrations were measured, and
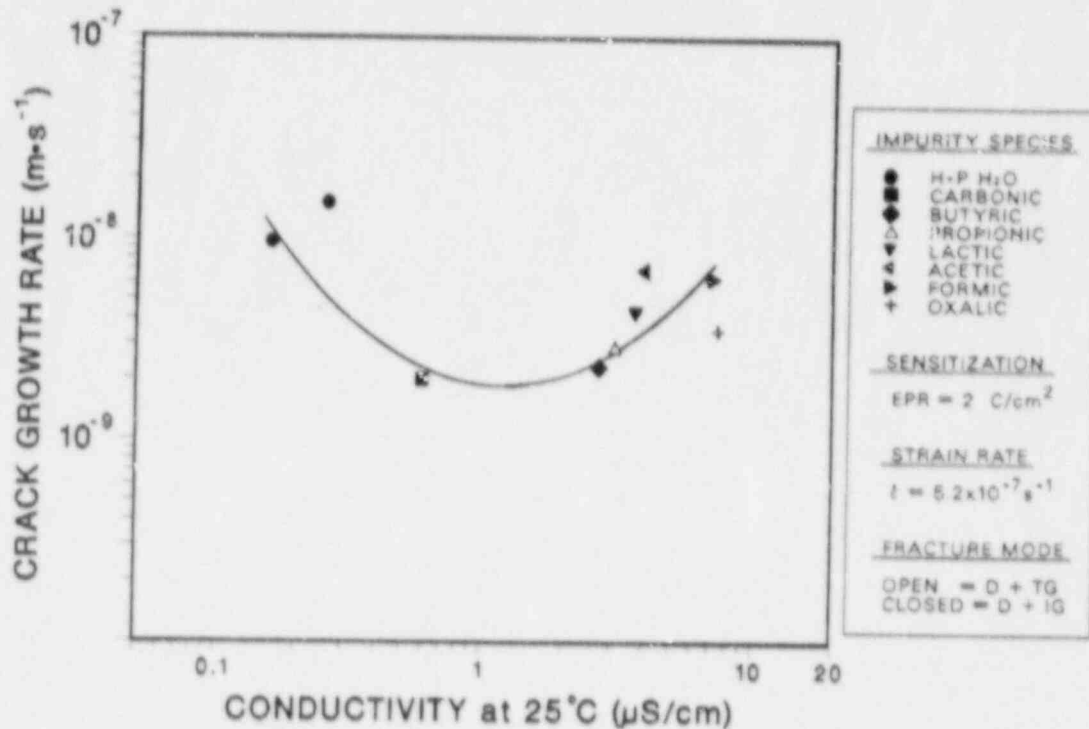
Fig. 26. Dependence of Crack Growth Rate of Lightly Sensitized Type 304 SS CERT Specimens at 289°C on Conductivity of the Feedwater Containing 0.2 ppm Dissolved Oxygen and 1.0 ppm of Several Carboxylic and Aliphatic Acids.

the values were only slightly lower than in the feedwater, viz., ~0.1 ppm by CHEMetrics analyses. This result is consistent with the ECP data for Type 304 SS, where the values range between ~0 and 100 mV(SHE), with the one exception noted above. Consequently, the decrease in IGSCC susceptibility in these experiments cannot be attributed solely to oxygen depletion in the water by reaction with the organic acids.

In a similar study,[48] the SCC behavior of sensitized Type 304 SS was determined in 275°C water containing formic, acetic, or oxalic acid at concentrations of 20, 26, or 39 ppm, respectively, and several dissolved oxygen concentrations (<0.005, 0.2, 0.6, and 8.0 ppm). Intergranular and ductile fractures occurred at the highest and lowest dissolved-oxygen concentrations, respectively, in the acid solutions; the times to failure of the CERT specimens in the impurity solutions were virtually the same as those in pure water at the respective oxygen levels. At the intermediate oxygen

concentration of 0.2 ppm, acetic acid increased IGSCC susceptibility, whereas
formic and oxalic acids inhibited IGSCC. Formic and oxalic acid additions to
the feedwater caused a significant negative shift (by ~400 mV) in the ECP of
Type 304 SS, which was not observed in the case of acetic acid. All of the
acids caused a decrease in the effluent dissolved-oxygen concentration. The
inhibiting effect of both formic and oxalic acids at the relatively high
concentrations in feedwater containing 0.2 ppm dissolved oxygen was attributed
to the large decrease in the corrosion potentials of the steel. It was
postulated that the negative shift in the ECP of the steel was caused by the
catalytic reduction of oxygen on the metal surface promoted by preferential
adsorption of the carboxylic acids intermediate products of their
decomposition.[48] In another investigation,[49] organic acids at even lower
concentrations (<~0.1 ppm) in oxy.   d water (~0.2 ppm) had a beneficial
effect on the SCC of sensitized Ty, 304 SS.

Since the redox potentials from the platinum electrode in Table 10
shifted, on the average, by ~430 mV in the negative directi   xcept for
acetic acid) without significant oxygen depletion in the wat.   is possible
that the organic acids interfered with the cathodic reduction of oxygen by
adsorption on the surface. Our previous results indicated that the
intergranular crack growth rate of sensitized Type 304 SS varies with the 1/4
power of the dissolved-oxygen concentration in high-purity water;[27]
consequently, the small difference between the inlet and effluent oxygen
concentrations (~0.25 versus ~0.1) cannot account for the decrease (by
approximately a factor of five) in the crack growth rates in the present
experiments.

The CERT results in Table 10 and in other investigations[48,49]
suggest that most of these organic acids or their probable decomposition
products (carbonate or bicarbonate ions) are not particularly deleterious
compared to that of sulfur species (viz., sulfate) at the same or lower
concentrations; nevertheless, the concentrations of these species should be
minimized because they contribute to the conductivity and decrease the pH of
the water, and consequently can hinder the detection of deleterious species
that are present at much lower concentrations. Fracture-mechanics crack-
growth-rate tests will be performed on sensitized Type 304 SS and

Type 316NG SS specimens to confirm the relatively innocuous or potentially beneficial effects of several of the organic acids on SCC in water at 289°C containing 0.2 ppm dissolved oxygen.

C. Environmentally Assisted Cracking of Ferritic Steels (J. Y. Park)

1. Introduction

Plain carbon steels are used extensively in PWR and BWR nuclear steam supply systems as piping and pressure vessel materials. The steels of interest for these applications include grades A106-Gr B and A333-Gr 6 for seamless pipe and A302-Gr B, A508-2, and A533-Gr B plate for pressure vessels. Although operating experience with ferritic steel components in reactor pressure boundaries is considerably better than with weld-sensitized austenitic stainless steels, instances of cracking of these steels have occurred in the U.S. and abroad.[50-58]

Ferritic steels become susceptible to TGSCC in high-temperature water containing dissolved oxygen in CERT[59-67] and fracture-mechanics tests.[67-73] There is some evidence of synergistic effects between dissolved oxygen and soluble copper compounds (viz., $CuCl_2$) as well as other impurities to produce susceptibility to SCC.[55,61] However, the ranges of dissolved oxygen and impurity concentrations that can lead to SCC in these materials remain relatively ill-defined. The objective of this work is to characterize the environmental and material conditions that can produce SCC susceptibility in these steels.

2. Technical Progress

Several ferritic steels (A333, A106, A155, A516, and A533B) used for piping and pressure vessels were obtained. These materials have been used in other U.S. NRC research programs at Battelle Columbus Laboratories and Materials Engineering Associates, Inc. (MEA) and have been well characterized in terms of mechanical properties. The chemical compositions of the materials are given in Table 11. Cylindrical gage length CERT and 1TCT fracture-mechanics-type specimens were fabricated from these materials.

Table 11. Chemical Composition of Ferritic Steels

Material	Heat No.	C	Mn	P	S	Si	Sn	Ni	Cr	Mo	V	Cu	Al
A533B	A5401	0.23	1.42	0.008	0.005	0.27	NA	0.70	0.12	0.56	NA	0.10	NA
A516 Grade 70	DP2-F34	-	-	-	-	-	-	-	-	-	-	-	-
A533B	XE5-M	0.22	1.42	0.018	0.008	0.18	NA	0.61	NA	0.56	NA	0.18	NA
A155-CK70	DP2-F26	0.13	0.80	0.009	0.027	0.25	0.007	0.13	0.13	0.40	NA	0.12	0.003
A106B	DP2-F29	0.28	0.82	0.010	0.023	0.18	0.011	0.11	0.14	0.20	0.002	0.088	0.019
A106B	DP2-F30	0.15	0.65	0.012	0.014	0.20	0.018	0.14	0.18	0.055	0.001	0.28	0.010

NA: not analyzed.

54

Existing CERT systems were modified to permit better control of dissolved-oxygen concentrations over the range 0.02 to 0.1 ppm. Stainless steel commences active general corrosion at dissolved-oxygen levels below 0.1 ppm, which in low-flow systems can lead to rapid depletion of the dissolved oxygen in the feedwater to levels below 0.02 ppm. To prevent this, stainless steel was replaced by titanium in all areas of the autoclave and water supply system in contact with high-temperature water.

A method was developed to electrically isolate the test specimens from the load train and autoclave, and electrodes for measurement of corrosion potentials of ferritic steel were fabricated. Baseline CERT tests were performed in high-purity water with 0.2 ppm dissolved oxygen at 289°C and strain rates of 2.5×10^{-7} and 1×10^{-6} s^{-1} for unnotched cylindrical specimens fabricated from A106B ferritic steel (Heat No. DP2-F30C). The results are given in Table 12.

At a strain rate of 1×10^{-6} s^{-1}, the specimen failed at a maximum load of 626 MPa with 17.6% total elongation and 16.5% reduction of area. As is shown in Fig. 27, a large (4-mm deep) nonductile transgranular crack developed on the fracture surface. The average crack propagation rate was 3×10^{-8} $m \cdot s^{-1}$. Significant pitting and an iron-rich, orange-colored corrosion product were observed on the fracture surface and on the specimen surface (Fig. 28) in the region of large plastic deformation. The pitting appeared to be associated with nonmetallic inclusions in the material. SEM-EDAX analysis will be performed on the corrosion products and the inclusions.

At a strain rate of 2.5×10^{-7} s^{-1}, the specimen showed slightly higher ductility: 29.2% total elongation, 39.3% reduction of area, and 632 MPa maximum load. The average crack propagation rate was 3×10^{-9} $m \cdot s^{-1}$, which is lower by an order of magnitude than that at the 1×10^{-6} s^{-1} strain rate. The pitting at the specimen surface was also less severe. Baseline CERT tests in high-purity oxygenated environments are continuing on the other ferritic materials.

Table 12. Results of CERT Tests on Ferritic Steels in 289°C Water Containing 0.2 ppm Dissolved Oxygen

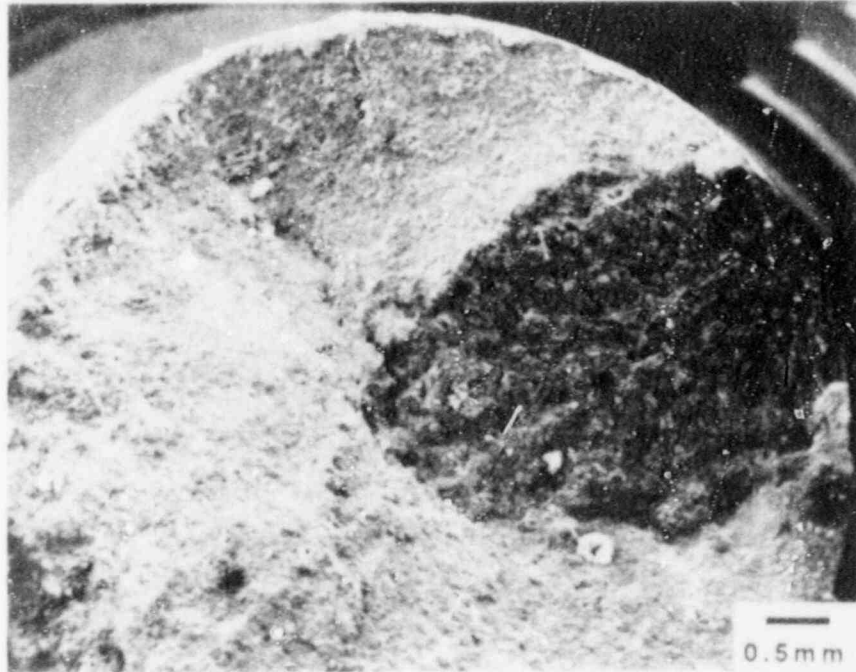| Material Heat No.	Specimen No.	$\dot{\varepsilon}$, s^{-1}	σ_{max}, MPa	t_f, h	$\Delta A/A_o$, %	ε_f, %	$\dot{a}_{av}$, $m \cdot s^{-1}$	ECP, mV(SHE)
A106B DP2-F30	30C-1	1×10^{-6}	626	47.7	16.5	17.6	3×10^{-8}	+50
"	30C-2	2.5×10^{-7}	632	291.7	39.3	29.2	3×10^{-9}	-20

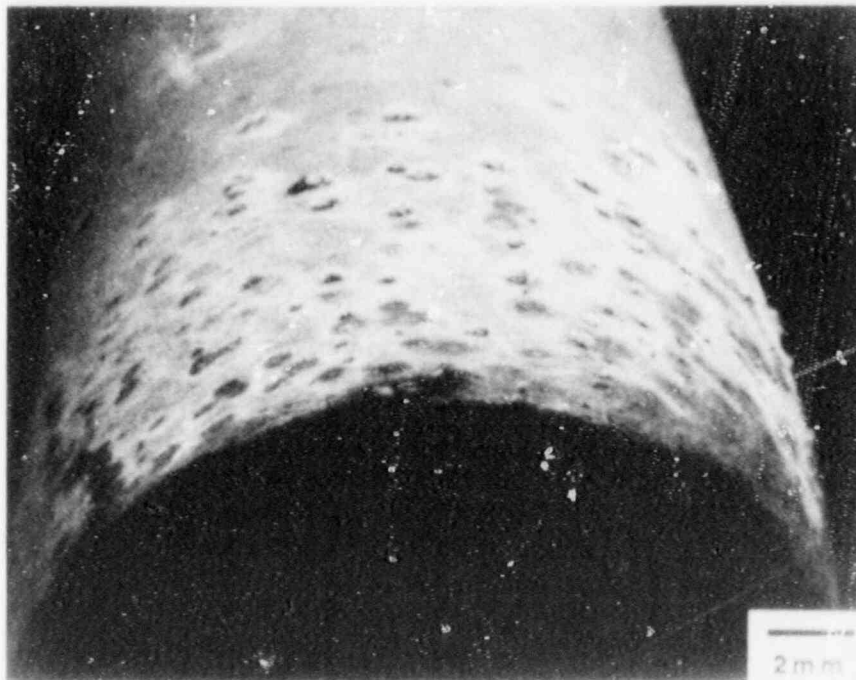Fig. 27. Fracture Surface of an A106B Ferritic Steel CERT Specimen.

Fig. 28. Pitting of Surface of the A106B Ferritic Steel CERT Specimen after Exposure to Water at 289°C with 0.2 ppm Dissolved Oxygen.

REFERENCES

1. W. E. Ruther, W. K. Soppet, and T. F. Kassner, in *Environmentally Assisted Cracking in Light Water Reactors: Annual Report, October 1982 - September 1983*, NUREG/CR-3806, ANL-84-36 (June 1984), pp. 119-124.

2. J. Y. Park, W. E. Ruther, T. F. Kassner, and W. J. Shack, *Stress Corrosion Crack Growth Rates in Type 304 Stainless Steel in Simulated BWR Environments*, J. Eng. Mater. Technol. 108, 20-25 (1986).

3. P. S. Maiya and W. J. Shack, in *Environmentally Assisted Cracking in Light Water Reactors: Semiannual Report, October 1985 - March 1986*, NUREG/CR-4667 Vol. II, ANL-86-37 (July 1986), pp. 19-26.

4. P. S. Maiya, in *Environmentally Assisted Cracking in Light Water Reactors: Semiannual Report, April - September 1986*, NUREG/CR-4667 Vol. III, ANL-87-37 (September 1987), pp. 11-18.

5. W. E. Ruther, W. K. Soppet, J. Y. Park, and T. F. Kassner, in *Environmentally Assisted Cracking in Light Water Reactors: Semiannual Report, April - September 1986*, NUREG/CR-4667 Vol. III, ANL-87-37 (September 1987), pp. 2-7.

6. M. T. Jones, *Reactor Technology Report*, Knolls Atomic Power Laboratory, No. KAPL 2000-11 (1960).

7. W. E. Ruther and S. Greenberg, *Corrosion of Steels and Nickel Alloys in Superheated Steam*, J. Electrochem. Soc. 111(10), 1116-1121 (1964).

8. W. E. Ruther, W. K. Soppet, and T. F. Kassner, in *Materials Science and Technology Division Light-Water-Reactor Safety Research Program: Quarterly Progress Report, October - December 1983*, NUREG/CR-3689 Vol.IV, ANL-83-85 Vol. IV (August 1984), pp. 75-87.

9. W. E. Ruther, W. K. Soppet, and T. F. Kassner, in *Light-Water-Reactor Safety Research Program: Quarterly Progress Report, January - March 1985*, NUREG/CR-4490 Vol.I, ANL-85-75 Vol. I (March 1986), pp. 43-49.

10. P. S. Maiya and W. J. Shack, in *Environmentally Assisted Cracking in Light Water Reactors: Semiannual Report, April - September 1985*, NUREG/CR-4667 Vol. I, ANL-86-31 (June 1986), pp. 16-26.

11. P. S. Maiya, in *Environmentally Assisted Cracking in Light Water Reactors: Semiannual Report, April - September 1986*, NUREG/CR-4667 Vol. III, ANL-87-37 (September 1987), pp. 7-11.

12. W. E. Ruther, W. K. Soppet, T. F. Kassner, and W. J. Shack, in *Environmentally Assisted Cracking in Light Water Reactors: Semiannual Report, October 1985 - March 1986*, NUREG/CR-4667 Vol II, ANL-86-37 (July 1986), p. 50.

13. W. E. Ruther, W. K. Soppet, and T. F. Kassner, in *Environmentally Assisted Cracking in Light Water Reactors: Semiannual Report, April - September 1985*, NUREG/CR-4667 Vol. I, ANL-86-31 (June 1986), pp. 46-5?

14. J. E. Hilliard, _Estimation of Grain Size by the Intercept Method_, Met. Prog. 4, 99 (1984).

15. P. S. Maiya and W. J. Shack, in _Light-Water-Reactor Safety Materials Engineering Research Programs: Quarterly Progress Report, January - March 1985_, NUREG/CR-4490 Vol. I, ANL-85-75 Vol.I (March 1986), pp. 16-24.

16. P. S. Maiya, "A Phenomenological Model for Stress Corrosion Cracking in Types 316NG and 316 Stainless Steel," in _Environmental Degradation of Materials in Nuclear Power Systems-Water Reactors_, Proc. of the 2nd Int. Symp., Monterey, CA, September 9-12, 1985, NACE (1986), pp. 12-17 and Discussion, p. 53.

17. F. P. Ford, _Mechanism of Environmental Controlled Crack Propagation in Systems Peculiar to Power Generation_, EPRI NP-1332-1 (August 1986).

18. A. F. Smith and G. B. Gibbs, _The Volume of Grain-Boundary Diffusion of Iron in 20Cr/25Ni/Nb Stainless Steel_, Metal Sci. J. 2, 47-50 (1968).

19. W. E. Ruther, W. K. Soppet, and T. F. Kassner, in _Materials Science and Technology Division Light Water Safety Research Program: Quarterly Progress Report, October - December 1983_, NUREG/CR-3689 Vol. IV, ANL-83-85 Vol. IV (August 1984), pp. 51-75.

20. J. Y. Park and W. J. Shack, in _Environmentally Assisted Cracking in Light Water Reactors: Semiannual Report, April - September 1986_, NUREG/CR-4667 Vol. III, ANL-87-37 (September 1987), pp. 26-29.

21. Private Communication, D. Gandy, EPRI NDE Center to W. J. Shack (March 1987).

22. E. F. Rybicki and R. B. Stonesifer, _Computation of Residual Stresses Due to Multipass Welds in Piping Systems_, J. Pressure Vessel Technol. 101, 149-154 (1979).

23. W. J. Shack, in _Environmentally Assisted Cracking in Light Water Reactors: Semiannual Report, April - September 1986_, NUREG/CR-4667 Vol. III, ANL-86-37 (September 1987), pp. 32-40.

24. N. R. Hughes and A. J. Gianuzzi, _Evaluation of Near-Term BWR Piping Remedies_, EPRI NP-1222 Vol. 2 (November 1979), pp. K 1-28.

25. W. H. Wolf and K. E. Perry, "Stress-Strain Determinations in the Mechanical Stress Improvement Process," _1986 Seminar on Countermeasures for Pipe Cracking in BWRs_, Palo Alto, CA, November 5-7, 1986.

26. W. E. Ruther, W. K. Soppet, and T. F. Kassner, in _Light-Water-Reactor Safety Materials Engineering Programs: Quarterly Progress Report, January - March 1985_, NUREG/CR-4490 Vol. I, ANL 85-75 Vol. I (March 1986), pp. 25-42.

27. W. E. Ruther, W. K. Soppet, and T. F. Kassner, in _Environmentally Assisted Cracking in Light Water Reactors: Semiannual Report, April - September 1985_, NUREG/CR-4667 Vol. I, ANL-86-31 (June 1986), pp. 27-41.

28. W. E. Bailey, M. O. Marlowe, and R. A. Proebstle, "Trends in BWR Fuel Performance," in _Light Water Reactor Fuel Performance_, Proc. Amer. Nucl. Soc. Topical Meeting, Orlando FL, April 21-24, 1985, Vol. 1, pp. 1-3 to 1-16.

29. M. O. Marlowe, J. S. Armijo, B. Cheng, and R. B. Adamson, "Nuclear Fuel Cladding Localized Corrosion," in _Light Water Reactor Fuel Performance_, Proc. Amer. Nucl. Soc. Topical Meeting, Orlando FL, April 21-24, 1985, Vol. 1, pp. 3-73 to 3-90.

30. A. K. Agrawal, J. F. Sykes, W. N. Stiegelmeyer, and W. E. Berry, "Pitting of Alloy 600 Steam Generator Tubes in Indian Point No. 3," in _Environmental Degradation of Materials in Nuclear Power Systems-Water Reactors_, Proc. of the Int. Symp., Myrtle Beach, SC, August 22-25, 1983, NACE (1984), pp. 223-242.

31. S. L. Harper, S. C. Inmann, P. L. Daniel, B. P. Miglin, and G. J. Theus, "Laboratory Evaluation of Steam Generator Tubes from Millstone Point Unit 2 and the Use of Pourbaix Diagrams to Infer Localized Corrosion Conditions," in _Environmental Degradation of Materials in Nuclear Power Systems-Water Reactors_, Proc. of the 2nd Int. Symp., Monterey, CA, September 9-12, 1985, NACE (1986), pp. 227-233.

32. S. J. Green and J. P. N. Paine, "Steam Generator Materials--Experience and Prognosis," in _Environmental Degradation of Materials in Nuclear Power Systems-Water Reactors_, Proc. of the Int. Symp., Myrtle Beach, SC, August 22-25, 1983, NACE (1984), pp. 53-68.

33. T. J. Zeh, G. O. Hayner, and A. K. Agrawal, "Intergranular Attack of Inconel 600 Tubes at Tube Support Plate Intersections in the Palisades Nuclear Power Plant," in _Environmental Degradation of Materials in Nuclear Power Systems-Water Reactors_, Proc. of the 2nd Int. Symp., Monterey, CA, September 9-12, 1985, NACE (1986), pp. 234-239.

34. D. D. Macdonald, A. K. Eghan, and Z. Szklarska-Smialowska, _Stress Corrosion Cracking of AISI 304 Stainless Steel in Oxygenated High Temperature Chloride Solutions Containing Cupric (Cu^{2+}) and Lead (Pb^{2+}) Ions_, Corrosion $\underline{41}$(8), 474-484 (1985).

35. F. P. Ford, "Stress Corrosion Cracking," in _Corrosion Processes_, R. N. Parkins, ed., Applied Science Publishers, New York, pp. 271-309 (1982).

36. D. A. Vermilyea, in _Proc. Intl. Conf. on Stress Corrsion Cracking and Hydrogen Embrittlement of Iron Base Alloys_, R. W. Staehle, J. Hochmann, R. D. McCright, and J. E. Slater, eds., NACE, Houston (1983), p. 208.

37. W. E. Ruther, W. K. Soppet, and T. F. Kassner, in _Environmentally Assisted Cracking in Light Water Reactors: Semiannual Report, April - September 1986_, NUREG/CR-4667 Vol III, ANL-87-37 (September 1987), pp. 40-50.

38. BWR Water Chemistry Guidelines, Prepared by the BWR Owners Group Water Chemistry Guidelines Committee, EPRI NP-3589 SR-LD (April 1985), pp. 3-1 to 3-9.

39. PWR Secondary Water Chemistry Guidelines, Revision 1, Prepared by the Steam Generator Owners Group Water Chemistry Guidelines Revision Committee, EPRI NP-5056-SR (March 1987), pp. 2-12 to 2-22 and 3-15 to 3-22.

40. H. D. Solomon, Transgranular, Granulated, and Intergranular Stress Corrosion Cracking in AISI 304 SS, Corrosion 40(9), 493-506 (1984).

41. W. E. Ruther, W. K. Soppet, and T. F. Kassner, in Environmentally Assisted Cracking in Light Water Reactors: Annual Report, October 1982 - September 1983, NUREG/CR-3806, ANL-84-36 (June 1984), pp. 101-108.

42. W. E. Ruther, W. K. Soppet, and T. F. Kassner, in Environmentally Assisted Cracking in Light Water Reactors: Annual Report, October 1983 - September 1984, NUREG/CR-4287 ANL-85-33 (June 1985), pp. 101-109.

43. W. E. Ruther, W. K. Soppet, and T. F. Kassner, Effect of Temperature and Ionic Impurities at Very Low Concentrations on Stress Corrosion Cracking of Type 304 Stainless Steel, Corrosion/85, Paper 102, Boston, MA, March 1985.

44. B. H. Dillman, R. A. Reed, and C. C. Lin, BWR Coolant Impurity Identification Study, Final Report, EPRI NP-4156 (August 1985).

45. B. H. Dillman, J. C. Elliot, R. A. Head, J. E. Osterle, and R. S. Tunder, Monitoring of Chemical Contaminants in BWRs, Final Report, EPRI NP-4134 (July 1985).

46. J. E. Richards and W. A. Byers, Industrywide Survey of PWR Organics, Final Report, EPRI NP-4698 (July 1986).

47. W. J. Shack, T. F. Kassner, P. S. Maiya, J. Y. Park, and W. E. Ruther, BWR Pipe Crack and Weld Overlay Studies, Nucl. Eng. Des. 89, 295-303 (1985).

48. G. Cragnolino and Z. Szklarska-Smialowska, Environmental Effects on Intergranular Stress Corrosion Cracking (IGSCC) of Sensitized Stainless Steel in High-Temperature Solutions, Final Report, EPRI NP-5364M (August 1987).

49. Private Communication, L. Ljungberg, ASEA-ATOM, Vasteras, Sweden, to T. F. Kassner (August 1987).

50. L. Frank, W. S. Hazelton, R. A. Herman, V. S. Noonan, and A. Taboada, Pipe Cracking Experience in Light-Water Reactors, NUREG-0679 (August 1980), pp. 7-9.

51. PWR Pipe Crack Study Group, Investigation and Evaluation of Cracking Incidents in Piping in Pressurized Water Reactors, NUREG-0691 (September 1980), pp. 2-12 to 2-23.

52. A. Goldberg, R. D. Streit, and R. G. Scott, _Evaluation of Cracking in Feedwater Piping Adjacent to Steam Generators in Nine Mile Point Pressurized Water Reactor Plants_, NUREG/CR-1603, UCRL-53000 (October 1980).

53. B. Vyas, C. J. Czajkowski, and J. R. Weeks, _Metallurgical Examination of Cracked Feedwater Pipes from Nine Pressurized Water Reactors_, Nucl. Technol. _55_, 525-537 (1981).

54. J. F. Enrietto, W. H. Bamford, and D. F. White, _Preliminary Investigation of PWR Feedwater Line Cracking_, Int. J. Pres. Ves. and Piping _9_, 345-358 (1981).

55. C. J. Czajkowski, _Investigation of Shell Cracking on the Steam Generators at Indian Point Unit No. 3_, NUREG/CR-3281, BNL-NUREG-51670 (June 1983).

56. J. Hickling and D. Blind, _Strain-Induced Corrosion Cracking of Low-Alloy Steels in LWR Systems--Case Histories and Identification of Conditions Leading to Susceptibility_, Nucl. Eng. Des. _91_, 305-330 (1986).

57. J. Jansky, D. Blind, and G. Katzenmeier, _Investigation of Piping Failure in the HRD Test Plant under Operational Conditions and the Influence of Oxygen Content_, Nucl. Eng. Des. _91_, 345-358 (1986).

58. C. J. Czajkowski, _Evaluation of Transgranular Cracking Phenomenon on the Indian Point No. 3 Steam Generator Vessels_, Int. J. Pres. Ves. and Piping _26_, 97-110 (1986).

59. H. Choi, F. H. Beck, Z. Szklarska-Smialowska, and D. D. Macdonald, _Stress Corrosion Cracking of ASTM A508 Cl 2 Steel in Oxygenated Water at Elevated Temperatures_, Corrosion _38_(3), 136-144 (1982).

60. T. Mizuno, S. Pednekar, Z. Szklarska-Smialowska, and D. D. Macdonald, "Corrosion and Stress Corrosion Cracking of Carbon Steel in Oxygenated, High-Purity Water at Elevated Temperatures," in _Environmental Degradation of Materials in Nuclear Power Systems-Water Reactors_, Proc. of the Int. Symp., Myrtle Beach, SC, August 22-25. 1983, NACE (1984), pp. 395-422.

61. C. J. Czajkowski, _Constant Extension Rate Testing of SA302 Grade B Material in Neutral and Chloride Solutions_, NUREG/CR-3614, BNL-NUREG-51736 (February 1984).

62. P. Hurst, D. A. Appleton, P. Banks and A. S. Raffel, _Slow Strain Rate Stress Corrosion Tests on A508-III and A533B in Deionized and PWR Water at 563K_, Corros. Sci. _25_, 651-671 (1985).

63. J. Congleton, T. Shoji, and R. N. Parkins, _The Stress Corrosion Cracking of Reactor Pressure Vessel Steel in High Temperature Water_, Corros. Sci. _25_, 633-650 (1985).

64. J. Kuniya, I. Masaoka, R. Sasaki, H. Itoh, and T. Okazaki, <u>Stress Corrosion Cracking Susceptibility of Low-Alloy Steels Used for Pressure Vessel Steels Used for Reactor Pressure Vessel in High- Temperature Oxygenated Water</u>, Trans. ASME J. of Press. Ves. Technol. <u>107</u>, 431-435 (1985).

65. K. Klemetti and H. Hanninen, "Effect of Electrochemical Potential on Stress Corrosion Cracking of Steel A508 in BWR Environment," in <u>Environmental Degradation of Materials in Nuclear Power Systems-Water Reactors</u>, Proc. of the 2nd Int. Symp., Monterey, CA, September 9-12, 1985, NACE (1986), pp. 70-76.

66. E. Lenz and N. Wieling, <u>Strain-Induced Cracking of Low-Alloy Steels in LWR Systems--Interpretation of Susceptibility by Means of a Three Dimensional (T, e, Dissolved Oxygen) Diagram</u>, Nucl. Eng. Des. <u>91</u>, 331-344 (1986).

67. T. Shoji, H. Nakajama, H. Tsuji, H. Takahashi, and T. Kondo, "Effect of Microstructure and Strength of Low-Alloy Steels on Cyclic Crack Growth in High-Temperature Water," in <u>Corrosion Fatigue: Mechanics, Metallurgy, Electrochemistry, and Engineering</u>, ASTM STP 801, T.W. Crooker and B. N. Leis, eds., ASTM (1983), pp. 256-286.

68. K. Torronen and M. Kemppainen, "Fractography and Mechanisms of Environmentally Enhanced Fatigue Crack Propagation of a Reactor Pressure Vessel Steel," in <u>Corrosion Fatigue: Mechanics, Metallurgy, Electrochemistry, and Engineering</u>, ASTM STP 801, T. W. Crooker and B. N. Leis, eds., ASTM (1983), pp. 287-318.

69. D. Weinstein, <u>BWR Environmental Cracking Margins for Carbon Steel Piping, Final Report</u>, EPRI-2406 (May 1982).

70. C. Amzallag, J. L. Bernard, and G. Slama, "Effect of Loading an Metallurgical Parameters on the Fatigue Crack Growth Rates of Pressure Vessel Steels in Pressurized Water Reactor Environment," in <u>Environmental Degradation of Materials in Nuclear Power Systems-Water Reactors</u>, Proc. of the Int. Symp., Myrtle Beach, SC, August 22-25, 1983, NACE (1984), pp. 727-745.

71. W. H. Bamford, "Environmental Cracking of Pressure Boundary Materials and the Importance of Metallurgical Considerations," in <u>Aspects of Fracture Mechanics in Pressure Vessels and Piping</u>, ASME PVP-<u>58</u>, S. S. Palusamy and S. G. Sampath, eds., (1982), pp. 209-228.

72. P. M. Scott and A. E. Truswell, "Corrosion Fatigue Crack Growth in Reactor Presure Vessel Steels in PWR Primary Water," in <u>Aspects of Fracture Mechanics in Pressure Vessels and Piping</u>, ASME PVP-<u>58</u>, S. S. Palusamy and S. G. Sampath, eds., (1982), pp. 271-301.

73. W. H. Cullen, "Effects of Loading Rate, Waveform, and Temperature on Fatigue Crack Growth Rates of RPV Steels," in <u>Aspects of Fracture Mechanics in Pressure Vessels and Piping</u>, ASME PVP-<u>58</u>, S. S. Palusamy and S. G. Sampath, eds., (1982), pp. 303-312.

Distribution for NUREG/CR-4667 Vol. IV (ANL-87-41)

Internal:

O. K. Chopra	J. F. Marchaterre	R. W. Weeks
H. M. Chung	K. Natesan	H. Wiedersich
L. W. Deitrich	J. Y. Park	ANL Patent Dept.
D. R. Diercks	W. E. Ruther	ANL Contract File
B. R. T. Frost	R. A. Scharping	ANL Libraries (2)
D. M. Gruen	W. J. Shack (5)	TIS Files (3)
T. F. Kassner (10)	W. K. Soppet	
D. S. Kupperman	E. M. Stefanski (2)	
P. S. Maiya	C. E. Till	
V. A. Maroni	R. A. Valentin	

External:

NRC, for distribution per R5 (315)
DOE-TIC (2)
Manager, Chicago Operations Office, DOE
R. Dalton, DOE-CH
R. B. Adamson, General Electric Co., Vallecitos Nuclear Center, P. O. Box 460, Pleasanton, CA 94566
P. L. Andresen, General Electric Corporate Research and Development, Schenectady, NY 12301
G. A. Arlotto, Office of Nuclear Regulatory Research, USNRC, Washington
D. Atteridge, Battelle Pacific Northwest Lab., P. O. Box 999, Richland, WA 99352
W. H. Bamford, Structural Materials Engineering, Westinghouse Electric Corp., WNES, Box 355, Pittsburgh, PA 15230
W. Berry, Battelle-Columbus Labs., 505 King Ave., Columbus, OH 43201
C. Y. Cheng, Office of Nuclear Reactor Regulation, USNRC, Washington
W. J. Collins, Office of Inspection and Enforcement, USNRC, Washington
G. Cragnolino, Brookhaven National Lab., Upton, NY 11973
R. M. Crawford, NUTECH Engineers, 225 N. Michigan Ave., Chicago, IL 60601
D. Cubicciotti, Electric Power Research Inst., P. O. Box 10412, Palo Alto, CA 94303
W. H. Cullen, Materials Engineering Assoc., Inc., 9700 B. George Palmer Highway, Lanham, MD 20706
J. C. Danko, U. Tennessee, Knoxville, TN 37996-2000
R. Duncan, Combustion Engineering, Inc., P. O. Box 500, Windsor, CT 06095
B. J. Elliot, Office of Nuclear Reactor Regulation, USNRC, Washington
M. Fox, APTECH, 1257 Elko Drive, Sunnyvale, CA 94089
Y. S. Garud, S. Levy, Inc., 1901 S. Bascom Ave., Campbell, CA 95008
F. Garzarolli, KWU, Hammerbackerstr. 12+14, Postface:3220, 8520 Erlangen, West Germany
B. M. Gordon, General Electric Co., 175 Curtner, San Jose, CA 95125
S. D. Harkness, Bettis Atomic Power Laboratory, P. O. Box 79, West Mifflin, PA 15122
D. O. Harris, 750 Welch Rd., Palo Alto, CA 94303
W. S. Hazelton, Office of Nuclear Reactor Regulation, USNRC, Washington
M. E. Indig, General Electric Co., P. O. Box 460, Pleasanton, CA 94566
H. S. Isaccs, Brookhaven National Laboratory, Upton, NY 11973
R. E. Johnson, Office of Nuclear Reactor Regulation, USNRC, Washington
R. H. Jones, Battelle Pacific Northwest Lab., P. O. Box 999, Richland, WA 99352
R. L. Jones, Electric Power Research Inst., P. O. Box 10412, Palo Alto, CA 94303

J. N. Kass, Lawrence Livermore National Lab., Livermore, CA 94550
P. M. Lang, Office of Converter Reactor Deployment, USDOE, Washington 20545
L. Ljungberg, ASEA-ATOM, Box 53, S-721 04, Vasteras, Sweden
C. D. Lundin, U. Tennessee, Knoxville, TN 37996-2200
D. D. Macdonald, SRI International, 333 Ravenswood Ave., Menlo Park, CA 94025
H. Metha, General Electric Co., 175 Curtner, San Jose, CA 95125
J. Muscara, Office of Nuclear Regulatory Research, USNRC, Washington
D. M. Norris, Electric Power Research Inst., P. O. Box 10412, Palo Alto, CA 94303
D. R. O'Boyle, Commonwealth Edison Co., P. O. Box 767, Chicago, IL 60690
R. A. Oriani, U. Minnesota, Minneapolis, MN 55455
R. A. Penny, New York Power Authority, 123 Main St., White Plains, NY 10601
S. Ranganath, General Electric Co., 175 Curtner, San Jose, CA 95125
E. J. Rowley, Commonwealth Edison Co., P. O. Box 767, Chicago, IL 60690
E. F. Rybicki, Dept. of Mechanical Engineering, U. Tulsa, Tulsa, OK 74110
P. M. Scott, UKAEA AERE-Materials Development Division, Harwell, Didcot,
  OX11 ORA, UK
C. Z. Serpan, Office of Nuclear Regulatory Research, USNRC, Washington
L. Shao, Office of Nuclear Regulatory Research, USNRC, Washington
P. G. Shewmon, Dept. of Metallurgical Engineering, Ohio State U., Columbus,
  OH 43210
R. D. Silver, Office of Nuclear Reactor Regulation, USNRC, Washington
S. Smialowska, Dept. of Metallurgical Engineering, Ohio State U., Columbus,
  OH 43210
L. J. Sobon, NUTECH Engineers, 6835 Via del Oro, San Jose, CA 95119
A. A. Solomon, School of Nuclear Engineering, Purdue U., West Lafayette, IN 47907
H. D. Solomon, General Electric, P. O. Box 43, Schenectady, NY 12301
D. M. Stevens, Lynchburg Research Center, Babcock & Wilcox Co., P. O. Box 239,
  Lynchburg, VA 24505
A. Taboada, Office of Nuclear Regulatory Research, USNRC, Washington
B. Tomkins, Risley Nuclear Power Development Labs., U.K. Atomic Energy Authority,
  Risley, Warrington, WA3 6AT, England
W. A. Van Der Sluys, Research & Development Division, Babcock & Wilcox Co.,
  5162 Beeson St., Alliance, OH 44601
E. Venerus, Knolls Atomic Power Laboratory, P. O. Box 1072, Schenectady, NY 12301
J. R. Weeks, Brookhaven National Lab., Upton, NY 11973
K. R. Wichman, Office of Nuclear Reactor Regulation, USNRC, Washington
F. Witt, Office of Nuclear Reactor Regulation, USNRC, Washington
A. W. Zeuthen, Long Island Lighting Co., P. O. Box 618, Wading River, NY 11792

1 REPORT NUMBER (Assigned by TIDC add Vol No if any)	NUREG/CR-4667 Vol. IV ANL-87-41

2 TITLE AND SUBTITLE

ENVIRONMENTALLY ASSISTED CRACKING IN LIGHT WATER
REACTORS: SEMIANNUAL REPORT, October 1986--March 1987

3 LEAVE BLANK

4 DATE REPORT COMPLETED	
MONTH	YEAR
January	1988

5 AUTHOR(S)

W. J. Shack, T. F. Kassner, P. S. Maiya,
J. Y. Park, and W. E. Ruther

6 DATE REPORT ISSUED	
MONTH	YEAR
February	1988

7 PERFORMING ORGANIZATION NAME AND MAILING ADDRESS (Include Zip Code)

Argonne National Laboratory
9700 South Cass Avenue
Argonne, Illinois 60439

8 PROJECT/TASK/WORK UNIT NUMBER

9 FIN OR GRANT NUMBER

A2212

10 SPONSORING ORGANIZATION NAME AND MAILING ADDRESS (Include Zip Code)

U.S. Nuclear Regulatory Commission
Office of Nuclear Regulatory Research
Washington, D. C. 20555

11a TYPE OF REPORT

Technical; Semiannual

b PERIOD COVERED (Inclusive dates)

October 1986--March 1987

12 SUPPLEMENTARY NOTES

13 ABSTRACT (200 words or less)

This progress report summarizes work performed by Argonne National Laboratory on
environmentally assisted cracking in light water reactors during the six months
from October 1986--March 1987.

14 DOCUMENT ANALYSIS - a KEYWORDS/DESCRIPTORS

Crack growth
Residual stress measurements
Sensitization

Stress corrosion cracking
Water chemistry
Weld overlays

b IDENTIFIERS/OPEN ENDED TERMS

15 AVAILABILITY STATEMENT	
Unlimited	
16 SECURITY CLASSIFICATION	
(This page)	
Unclassified	
(This report)	
Unclassified	
17 NUMBER OF PAGES	
63	
18 PRICE	